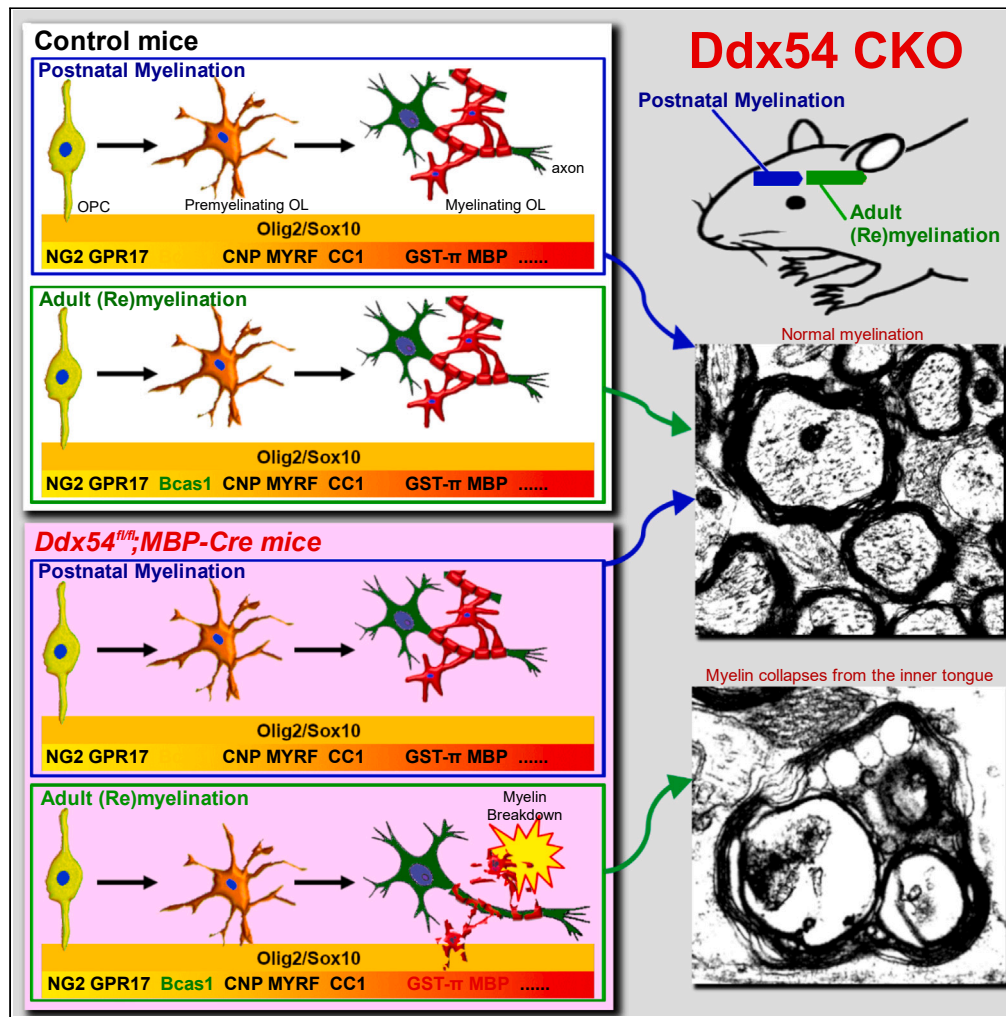**Article**

Lethal adulthood myelin breakdown by oligodendrocyte-specific Ddx54 knockout

Hiroaki Oizumi,
Yuki Miyamoto,
Chika Seiwa, ...,
Kazushige
Mizoguchi, Junji
Yamauchi, Hiroaki
Asou

hirokoma@h.email.ne.jp

Highlights

Ddx54 KO in
oligodendrocytes induces
lethal myelin breakdown
only in adulthood

Myelin collapses from
inner tongue without
peripheral infiltrate in
Ddx54 KO mice

Ddx54 KO scarcely affects
oligodendrocyte
differentiation or
postnatal myelination

Ddx54 KO mice represent
a new model of
remyelination failure

CellPress
OPEN ACCESS

Article

Lethal adulthood myelin breakdown by oligodendrocyte-specific Ddx54 knockout

Hiroaki Oizumi,[1,7] Yuki Miyamoto,[2,3,7] Chika Seiwa,[4] Masahiro Yamamoto,[1,8,*] Nozomu Yoshioka,[5] Seiichi Iizuka,[1] Tomohiro Torii,[6] Katsuya Ohbuchi,[1] Kazushige Mizoguchi,[1] Junji Yamauchi,[2,3] and Hiroaki Asou[4]

SUMMARY

Multiple sclerosis (MS) is a leading disease that causes disability in young adults. We have previously shown that a DEAD-box RNA helicase Ddx54 binds to mRNA and protein isoforms of myelin basic protein (MBP) and that Ddx54 siRNA blocking abrogates oligodendrocyte migration and myelination. Herein, we show that MBP-driven Ddx54 knockout mice (*Ddx54 fl/fl;MBP-Cre*), after the completion of normal postnatal myelination, gradually develop abnormalities in behavioral profiles and learning ability, inner myelin sheath breakdown, loss of myelinated axons, apoptosis of oligodendrocytes, astrocyte and microglia activation, and they die within 7 months but show minimal peripheral immune cell infiltration. Myelin in *Ddx54^{fl/fl};MBP-Cre* is highly vulnerable to the neurotoxicant cuprizone and Ddx54 knockdown greatly impairs myelination *in vitro*. Ddx54 expression in oligodendrocyte-lineage cells decreased in corpus callosum of MS patients. Our results demonstrate that Ddx54 is indispensable for myelin homeostasis, and they provide a demyelinating disease model based on intrinsic disintegration of adult myelin.

INTRODUCTION

Multiple sclerosis (MS) is the most frequent inflammatory disease of the central nervous system (CNS) and is characterized by demyelination and oligodendrocyte loss.[1] Although much progress has been made in developing immunomodulatory treatments to reduce myelin damage and inflammation, they cannot rescue the eventual failure of remyelination or accumulation of neuronal damage that occurs as MS progresses.[2,3] Conventionally, the failure of remyelination has been attributed to defects in oligodendrocyte progenitor cell (OPC) recruitment toward the demyelinated lesions and/or to their incapacity to differentiate and remyelinate. However, this view has been challenged by recent findings in experimental animals[4–7] and MS patients[8,9] concerning the mature oligodendrocytes' unexpected variety, longevity, and major contribution to adult myelin repair/adaptation. In addition, because MS commonly affects young adults between the ages 20–40 years, defects in myelination in adulthood (i.e., involving myelin repair, adaptive myelination, and/or myelin remodeling) may also be involved in MS pathogenesis.[10,11] Extensive reexamination of the role and mechanism of action of oligodendrocyte lineage cells in myelination, especially in adulthood, is warranted.

We have previously shown that the DEAD-box RNA helicase Ddx54 is expressed in a proportion of oligodendrocyte-lineage cells from the embryonic period (e.g., embryonic day 9 in rats) to senile stage, which bind to mRNA and protein isoforms of myelin basic protein (MBP), thereby enhancing the activity of MBP promoter and triggering the nuclear translocation of the 21.5 kDa MBP isoform.[12] Furthermore, knockdown of Ddx54 by injection of an adenoviral vector encoding a small interfering RNA (siRNA) in mouse brain specifically decreased the 21.5 kDa MBP isoform, and prevented axon myelination in the corpus callosum (CC) by halting MBP intrusion into CC at the subplate layer.[13]

In the present study, to investigate the role of Ddx54 in myelin biology, we generated an oligodendrocyte-specific Ddx54 knockout mouse, *Ddx54^{fl/fl};MBP-Cre*, using an MBP promoter-driven Cre-loxP system. The mice were normally born and grown up except for slight temporal retardation of postnatal myelination: myelination was recovered until the age of 2 months. However, the behavioral abnormality began to be observed since the age of 4 months, and demyelination, characterized by scattered drop off of myelinated

[1]Tsumura Kampo Laboratories, Tsumura & Co, Ami, Ibaraki 300-1192, Japan

[2]Department of Pharmacology, National Research Institute for Child Health and Development, Setagaya-ku, Tokyo 157-8535, Japan

[3]Laboratory of Molecular Neuroscience and Neurology, Tokyo University of Pharmacy and Life Sciences, Hachioji, Tokyo 192-0392, Japan

[4]Glovia Myelin Research Institute, Tsurumi-ku, Yokohama, Kanagawa 230-0046, Japan

[5]Division of Neurobiology and Anatomy, Graduate School of Medical and Dental Sciences, Niigata University, Chuo-ku, Niigata 951-8510, Japan

[6]Laboratory of Ion Channel Pathophysiology, Graduate School of Brain Science, Doshisha University, Kyotanabe, Kyoto 610-0394, Japan

[7]These authors contributed equally

[8]Lead contact

*Correspondence: hirokoma@h.email.ne.jp

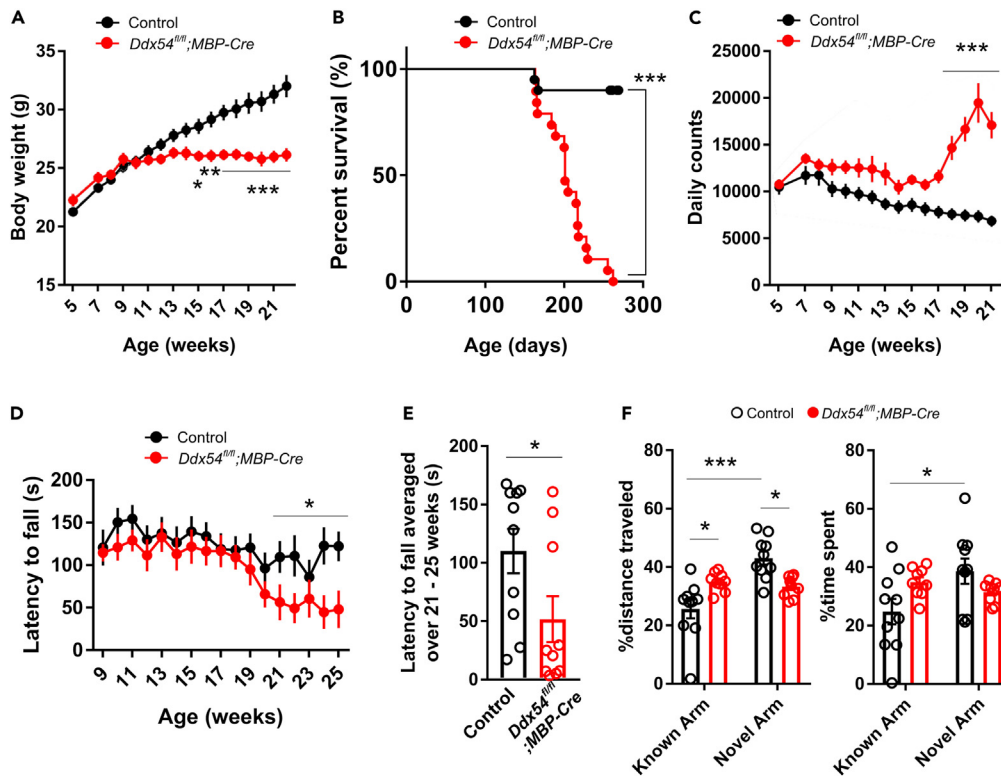https://doi.org/10.1016/j.isci.2023.107448

Figure 1. *Ddx54^{fl/fl};MBP-Cre* mice show lethality, behavioral abnormality and learning deficits

(A) Body weight of Control and *Ddx54^{fl/fl};MBP-Cre* mice (n = 10 mice, *$p < 0.05$ on day 15, **$p < 0.01$ on day 16, ***$p < 0.001$ on days 17–21).

(B) Survival curves of Control and *Ddx54^{fl/fl};MBP-Cre* mice (n = 20 mice, ***$p < 0.0001$).

(C) Locomotor activity in their home cage environment began to increase at the age of approximately 4 months (n = 10 mice, ***$p < 0.001$, on days 18–21).

(D) *Ddx54^{fl/fl};MBP-Cre* mice demonstrate impaired motor learning on the rotarod starting at age 5 months (n = 10 mice, *$p < 0.001$, on days 21, 22, 24, 25).

(E) Latency from 21 to 25 weeks decreased in *Ddx54^{fl/fl};MBP-Cre* mice compared with Control mice (n = 10 mice, *$p < 0.05$).

(F) In the Y-maze test, the percentage of the mouse's exploration distance and that of time spent in the novel arm increased in Control mice, indicating functional spatial working memory. *Ddx54^{fl/fl};MBP-Cre* mice did not show such increases, and the lack of change resulted in significantly different values from those of Control in the percentage of distance traveled in the known and novel arms (n = 10 mice, *$p < 0.05$, ***$p < 0.001$).

Data except for (A) are represented as mean ± s.e.m. Statistical analysis methods were Bonferroni's multiple comparisons test for (A, C, D, and F), Log rank test for (B) and Mann Whitney test for (E).

axon-oligodendrocyte bundles rather than hypomyelination, as well as learning deficits, were evident at age 5–6 months, and all mice died within 7 months. Remyelination after cuprizone-induced demyelination does occur but with serious malformation of myelin sheath. The present results suggest that Ddx54 is indispensable for adult myelin homeostasis and may provide a model of MS and other demyelinating diseases.

RESULTS

Ddx54^{fl/fl};MBP-Cre mice gradually develop behavioral aberration and learning deficit

An oligodendrocyte-specific Ddx54 knockout mouse, *Ddx54^{fl/fl};MBP-Cre*, using an MBP promoter-driven Cre-loxP system was generated by the scheme shown in Figure S1. The mice were apparently normal at birth but body weight gain stopped when they reached 3 months (Figure 1A) and they developed generalized seizures at 5–6 months. The clinical onset was similar in all mice with the first sign being mild and transient generalized tonic convulsion developing ataxia, episodes of immobility, hiccup-like movement, and bouncing, which worsened over 1–2 weeks with exacerbations and remissions in some mice. Some

began to die at age 5 months and all died within 7 months; the median survival time was 201 days (Figure 1B). Macroscopic and histopathological examination of necropsied 6-month-old mice revealed renal changes that were relatively mild and thought not to be the cause of convulsions (see "macroscopic observation, histopathology, and Luxol fast blue staining" section in STAR methods). Locomotor activity increased beginning at age 9 weeks and rapidly decreased as death approached (Figure 1C). Deficits of motor coordination and learning/memory, estimated by rotarod test and Y-maze test, respectively, have been observed (Figures 1D to 1F).

Adult onset myelin breakdown in *Ddx54*$^{fl/fl}$*;MBP-Cre* mice

Immunohistochemistry performed at postnatal day 10 (P10) revealed mild hypomyelination indicated by a decrease in the number of myelinated axons, increase in G-ratio, and decrease in MBP and 2′,3′-cyclic nucleotide-3′-phosphodiesterase (CNPase) intensity and reduced GFAP and Iba1 signal intensity (Figures S2A–S2Q). However, these parameters caught up to the normal within 2 months (2 Mo) (Figures S3A–S3Q). No histological aberrations were observed at both periods. The results of quantitative RT-PCR of total RNAs prepared from whole brain homogenate at P10 and 2 Mo indicate the expression of genes related to myelination and oligodendrocyte differentiation (i.e., Olig2, Sox10, GPR17, Bcas1, MYRF1, MBP, CNPase, and glutathione S-transferase-π (GST-π) mRNAs) were not significantly different between *Ddx54*$^{fl/fl}$*;MBP-Cre* and control mice (Figures S4A and S4B). Only the expression of the targeted gene Ddx54 showed a clear decrease in *Ddx54*$^{fl/fl}$*;MBP-Cre* mice compared to control mice. These data suggest that Ddx54 knockdown resulted in only slight changes to oligodendrocyte differentiation and myelination. Specifically, the changes observed at P10 were temporal and indicate slight retardation rather than inhibition.

At 5 months of age, when Ddx54 knockout mice began to die, minor changes in Olig2$^+$ cell number (decrease) and Iba1 intensity (increase) were observed with no evident alteration in MBP and CNPase or the percentage of myelinated axons (Figure S5). At 6.5 months (6.5 Mo), which closely corresponds to median survival time, numerous scattered spongiform degenerative changes in the brain appeared with a concomitant decrease in MBP immunosignals (Figure 2). LFB staining of the CC (Figures 2A and 2B), cerebellum, and brainstem (Figures 2C and 2D) together with MBP staining of the CC (Figures 2E and 2F) were performed. Apoptosis in the CC was markedly increased at 6.5 Mo (Figures 2G and 2H). Even at 5 Mo, high-power microscopy of MBP immunohistochemistry sections revealed the presence of enlargement and curving of spaces where sheaths and axons exfoliated (Figure 2I) in some mice.

To investigate the time course of lesion development, brain sections at 4 Mo, 5 Mo, and 6.5 Mo were examined in detail by electron microscopy. At 4 Mo, no aberration in myelin was evident (data not shown). By contrast, at 5 Mo, the individual differences were significant. Some mice had large, empty extracellular cavities generated by drop off of bunches of axons and myelinating oligodendrocytes, which left traces such as myelin loop and other intracellular organelle debris (Figure 2J, markers 1 to 4). In such mice, numerous myelin balloons of various sizes were observed (Figures 2J and 2K, the left panel). For example, a large myelin balloon is shown in Figure 2J, marker 5. This balloon presumably arose by apposition of the outer faces of the myelin-forming plasma membrane from adjacent myelin sheaths.[14] Myelin vacuolization (Figure 2J, marker 6) with normal or compressed axons (Figure 2J, marker 7) were also frequently shown (Figure 2K, the right panel). Both myelin vacuolization and the formation of myelin balloons are recognized hallmarks of demyelination, suggesting the mice had undergone demyelination.[14,15] In addition, myelin duplications containing tubular structures exfoliated/dissolved from the inner oligodendroglial loop were observed despite a well-preserved outer myelin sheath (e.g., Figure 2J, markers 8 and 9). These findings clearly indicate that myelin breakdown occurred essentially from the cytoplasmic side of the myelin sheath at the inner tongue. Axons that had accumulated electron-dense debris from disrupted cytoplasmic organelles inside the intact myelin (e.g., Figure 2J, marker 10) were also found, although the mechanism for the formation of such lesions remains unclear. All these phenotypes, especially the latter two, resemble those reported for MS brains.[16–20] Electron micrograph of the brain from all 6.5 Mo mice showed a number of demyelinated axons and activated macrophages (Figures 2L and 2M). However, as with the 5 Mo mice, the lesions were discrete with the surrounding cells and extracellular space appearing normal with no peripheral infiltrating lymphocytes.

Analysis of expression of glial markers and Ddx54 in *Ddx54*$^{fl/fl}$*;MBP-Cre* mice

The balance of neuronal and glial cell populations in the CC at 6.5 Mo did not show a significant difference between control and *Ddx54*$^{fl/fl}$*;MBP-Cre* mice. More than 80% were Olig2$^+$, CC1$^+$, or NG2$^+$ cells,
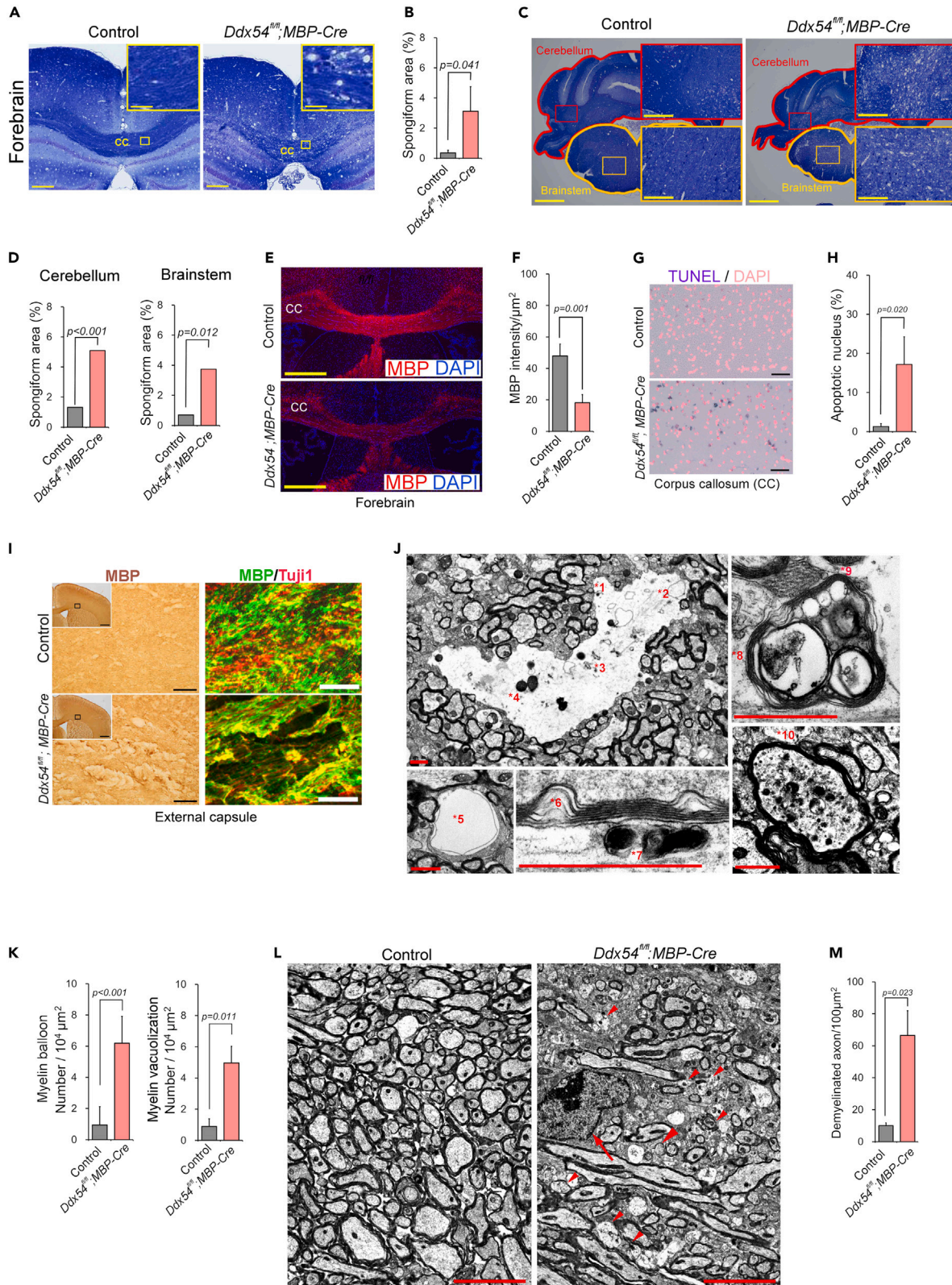
Figure 2. Ddx54 knockout induces scattered drop off of oligodendrocyte-myelinated axons complex and myelin degeneration with minimal effect on surrounding cells and spaces

(A) Luxol fast blue (LFB) and cresyl violet staining of a coronal section of the forebrain shows numerous spongiform changes in the corpus callosum (CC) of *Ddx54*$^{fl/fl}$*;MBP-Cre* mice at age 6.5 months (6.5 Mo). Scale bars represent 250 μm (inlet 30 μm).

(B) Quantification of the percentage (n = 4 mice) of spongiform area (white spaces) in the CC.

(C) LFB and cresyl violet staining of a coronal section of the cerebellum and brainstem shows numerous spongiform changes in *Ddx54*$^{fl/fl}$*;MBP-Cre* mice at 6.5 Mo. Scale bars represent 1000 μm (inlet 250 μm).

(D) Quantification of the percentage (n = 3 mice) of spongiform area in the cerebellum and brainstem.

(E) Immunohistochemical MBP staining shows decreased MBP levels in *Ddx54*$^{fl/fl}$*;MBP-Cre* mice at 6.5 Mo. Scale bars represent 500 μm.

(F) Quantification of MBP immunofluorescence (n = 4 mice) in the CC.

(G) TUNEL staining shows numerous apoptotic nuclei in the CC of *Ddx54*$^{fl/fl}$*;MBP-Cre* mice at 6.5 Mo. Scale bars represent 50 μm.

(H) Quantitation of apoptotic nuclei (n = 4 mice).

(I) High-power microscopy of MBP immunofluorescence shows enlargement and curving of spaces in the external capsule, and in certain areas, sheaths and axons exfoliated in *Ddx54*$^{fl/fl}$*;MBP-Cre* mice even at 5 months of age (5 Mo). Left panel: 3,3'-diaminobenzidine detection of horseradish peroxidase labeling. Scale bars represent 50 μm (inlet: 500 μm). Right panel: fluorescent labeling. Scale bars represent 40 μm.

(J) Electron microscopy of lesions in *Ddx54*$^{fl/fl}$*;MBP-Cre* mice at 5 Mo. A representative large empty extracellular cavity generated by drop off of a bunch of axons and myelinating oligodendrocytes (*1), leaving traces such as "ghost" axons having only an outer myelin loop (*2), fragments of endoplasmic reticulum (*3), and disintegrated mitochondria (*4). A large fluid-containing myelin balloon (*5), myelin vacuolization (*6), and large membranous inclusions with the cytoplasm of axons (*7) were frequently observed. Axons with myelin reduplication (*8) containing a tubular structure (*9) made like as inflating balloons from cytoplasmic-side of myelin at the inner tongue despite a well-preserved outer myelin sheath, and axons with accumulating electron-dense debris of cytoplasmic organelles despite having intact myelin (*10) have also been observed. These features have also been reported in multiple sclerosis patients (See results). All scale bars represent 1 μm.

(K) Quantification of myelin balloons (n = 13 fields counted from a set of littermate mice) and myelin vacuolization (n = 3 fields counted from a set of littermate mice).

(L) Electron microscopy of lesions in *Ddx54*$^{fl/fl}$*;MBP-Cre* mice at 6.5 Mo. A number of myelin balloons, demyelinated axons (arrowhead) and a macrophage (arrow) are shown. Scale bars represent 5 μm.

(M) Quantification of demyelinated axons (n = 3 sets of littermate mice).

Data in (B, D, F, H, K and M) are represented as mean ± s.d. and statistical comparisons were made using unpaired Student's *t* test.

corresponding to oligodendrocyte-lineage cells, with the remnant were GFAP$^+$ astrocytes, Iba1$^+$ microglia, and NeuN$^+$ neuronal cells (Figures 3A and 3B). However, the intensity of GFAP and Iba1 signals increased (Figures 3C, 3D, 3G, and 3H) suggesting the activation of existing astrocytes and microglia. The ratio of C3d$^+$ A1 astrocytes (Figures 3E and 3F) and iNOS$^+$ M1 microglia increased and Arg1$^+$ M2 microglia decreased (Figures 3I and 3J), indicating the onset of neuroinflammation.

To evaluate the effect of Ddx54 knockout on oligodendrocyte lineage cells, various markers of oligodendrocyte differentiation (i.e.,Olig2, NG2, GPR17, Sox10, MYRF1, CC1, Glutathione S-transferase-π (GST-π) and Bcas1) were immunostained using P10 (Figures S6A–S6D) 2 Mo (Figures S6E–S6H) and 6.5 Mo (Figure 4) brain sections. In the *Ddx54*$^{fl/fl}$*;MBP-Cre* CC at 6.5 Mo, the number of Olig2$^+$ nuclei decreased while the number of Sox10 remained unchanged (Figure 4B). Bcas1 is a marker of premyelinating oligodendrocytes, which is reported useful for identification of newly generated oligodendrocytes in the adult.[21] The level of Bcas1$^+$ cells increased in *Ddx54*$^{fl/fl}$*;MBP-Cre* CC at 6.5 Mo (Figure 4B). Bcas1$^+$ and CC1$^+$ areas increased (Figure 4C) and GST-π$^+$ cell number and area decreased while those of NG2$^+$, GPR17$^+$, and MYRF1$^+$ did not change (Figures 4D and 4E). At P10 and 2 Mo, there was no difference in the expression of these markers between *Ddx54*$^{fl/fl}$*;MBP-Cre* and the control mice (Figure S6) and virtually no Bcas1 signal could be detected.

The decrease in the level of Ddx54 protein in *Ddx54*$^{fl/fl}$*;MBP-Cre* mice was verified by immunoblot analysis using cortex, CC and cerebellum homogenates (Figure S1C). The decrease in Ddx54 mRNA is shown by quantitative RT-PCR using brain homogenate (Figure S4). Immunohistochemical analysis (Figure S7A) indicated that the expression of Ddx54 protein was not limited to oligodendrocyte-lineage cells as previously reported.[22] Olig2$^+$, CC1$^+$, or NG2$^+$ cells represent virtually all oligodendrocyte-lineage cells (Figure 4A). Ddx54 is expressed in a proportion of astrocytes and microglia (Figure S7C) as well as in Olig2$^+$, CC1$^+$ or NG2$^+$ cells (Figure S7B). The level of expression of Ddx54 in *Ddx54*$^{fl/fl}$*;MBP-Cre* mice decreased in oligodendrocyte-lineage cells (Figure S7D), showed no significant change in astrocytes (Figure S7E), and increased in microglia (Figure S7F) by comparison to the control mice. Accordingly, the percentage of Ddx54 signals expressed by oligodendrocyte-lineage cells to the total Ddx54 signals decreased in *Ddx54*$^{fl/fl}$*;MBP-Cre* mice (Figure S7G). Taken together, these data indicate the level of Ddx54 expression decreased specifically in oligodendrocyte-lineage cells. Moreover, there appeared to be a concomitant upregulation of Ddx54 expression in both astrocytes and microglia.
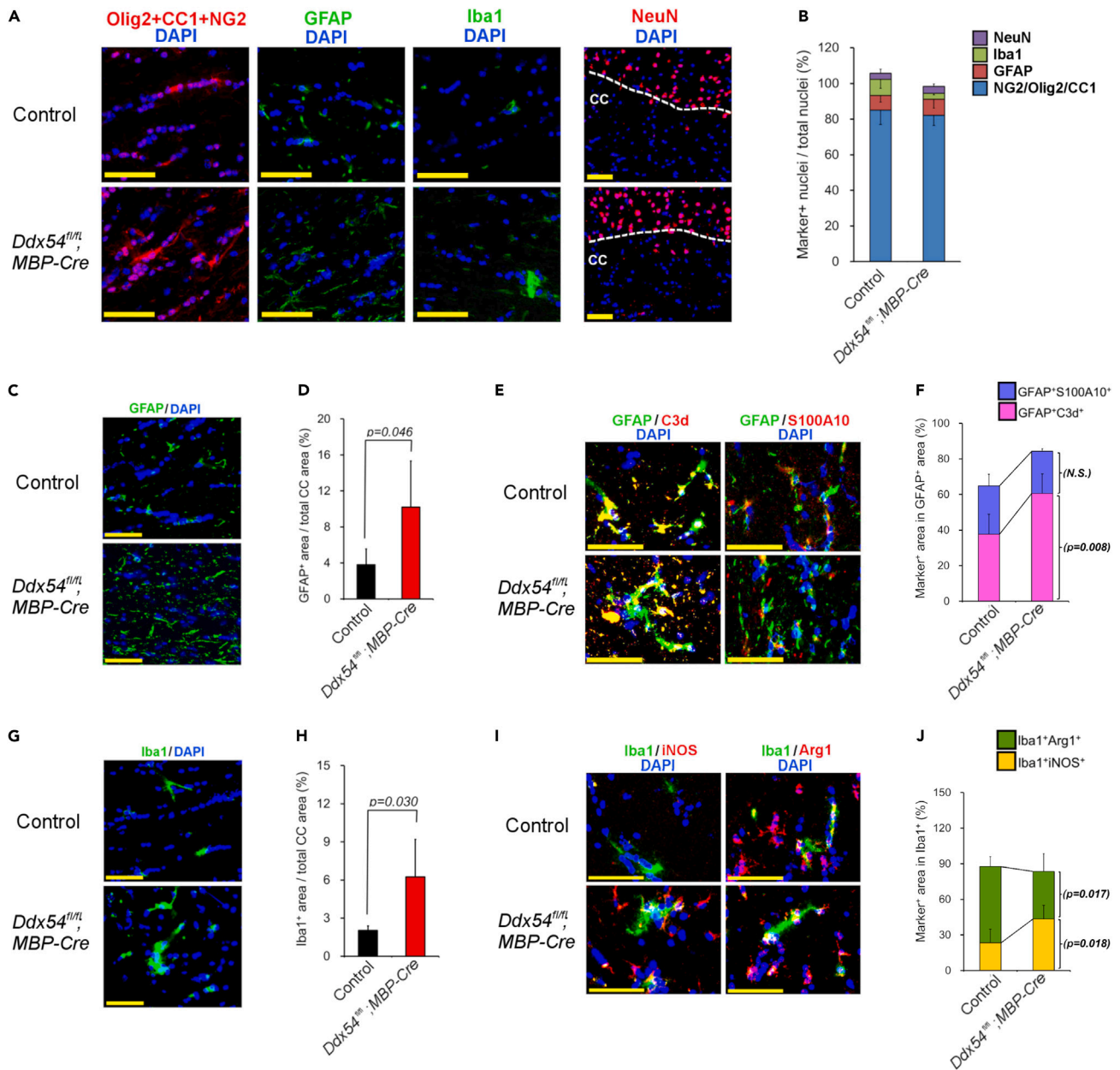
Figure 3. Astrocyte and microglia activation in the CC of Ddx54 fl/fl; MBP-Cre mice at 6.5 Mo

(A) Representative images of immunostaining by Olig2+CC1+NG2 (an antibody mixture for labeling oligodendrocyte-lineage cells), GFAP (for labeling astrocytes), Iba1 (for labeling microglia) or NeuN (for labeling neuronal cells). Scale bars represent 50 μm.

(B) Cell population analysis shows that the percentages of oligodendrocyte-lineage cells, astrocytes, microglia, and neuronal cells do not differ between control and *Ddx54^{fl/fl};MBP-Cre* mice (mean ± s.d., *n* = 4–6 mice).

(C) Representative images of immunostaining by GFAP. Scale bars represent 50 μm.

(D) Quantification of GFAP immunofluorescence shows activation of astrocytes in *Ddx54^{fl/fl};MBP-Cre* mice (mean ± s.d., n = 3 mice).

(E) Representative images of immunostaining by GFAP/C3d or GFAP/S100A10. Scale bars represent 50 μm.

(F) Subpopulation analysis of astrocytes shows an increase in C3d$^+$ A1 area in *Ddx54^{fl/fl};MBP-Cre* mice (mean ± s.d., n = 3 mice).

(G) Representative images of immunostaining by Iba1. Scale bars represent 50 μm.

(H) Quantification of Iba1 immunofluorescence shows activation of microglia in *Ddx54^{fl/fl};MBP-Cre* mice (mean ± s.d., n = 3 mice).

(I) Representative images of immunostaining of Iba1/iNOS or Iba1/Arg1 immunostaining activation of astrocytes in *Ddx54^{fl/fl};MBP-Cre* mice (mean ± s.d., n = 3 mice). Scale bars represent 50 μm.

(J) Subpopulation analysis of microglia shows an increase in iNOS$^+$ M1 cells and decrease in Arg1$^+$ M2 cells in *Ddx54^{fl/fl};MBP-Cre* mice (mean ± s.d., n = 3 mice). Statistical analysis was performed using Student's *t* test. N.S., not significant.
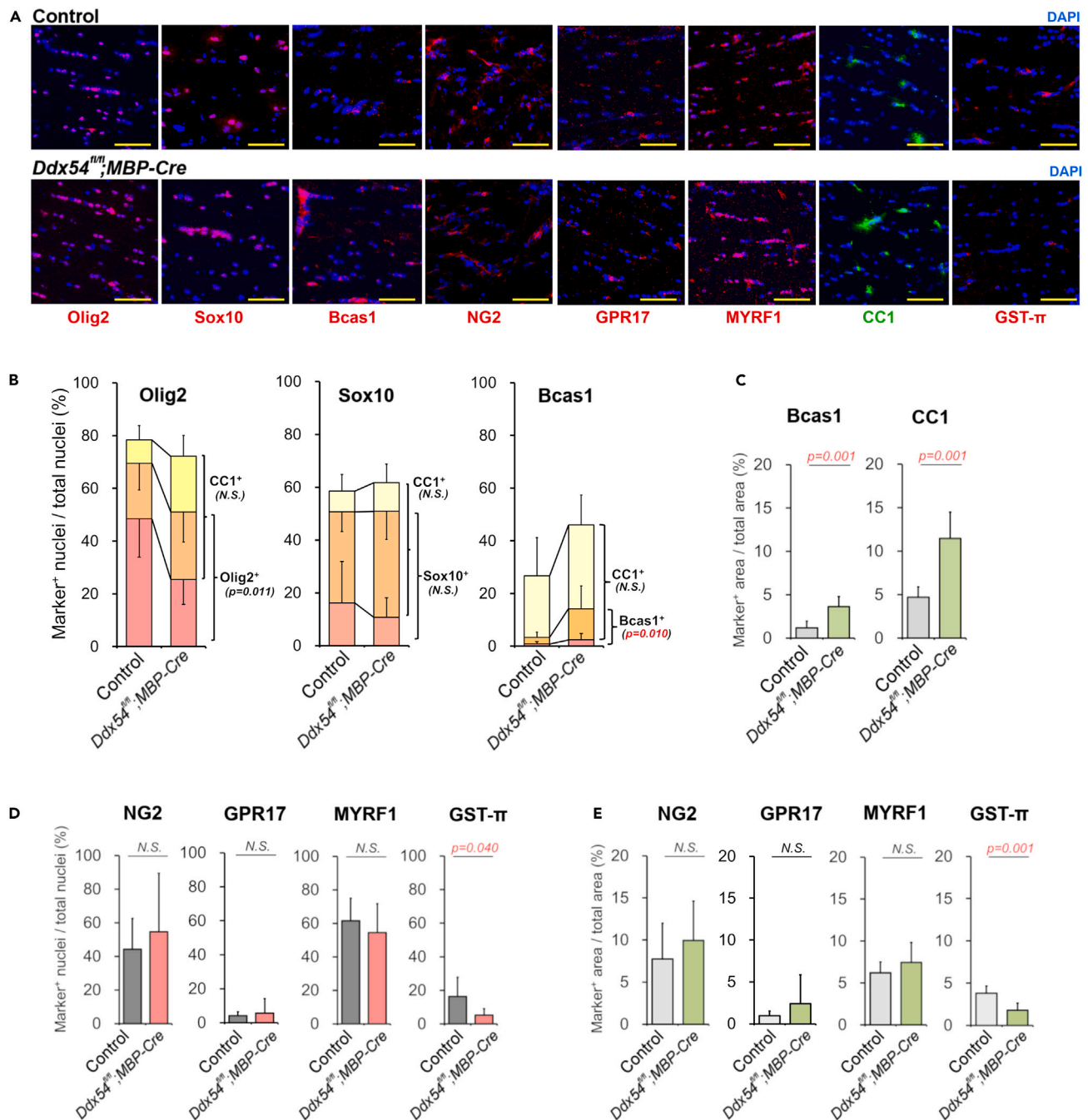
Figure 4. Cell marker analysis of the CC in *Ddx54*fl/fl*/;MBP-Cre* mice at age 6.5 Mo shows the disorder at a very late stage of oligodendrocyte maturation and induction of compensatory activation of oligodendrocyte differentiation

(A) Representative images of immunostaining by oligodendrocyte differentiation markers. Scale bars represent 50 μm.

(B) Subpopulation analysis by Olig2, Sox10, Bcas1 and CC1 shows a decrease in Olig2$^+$ cells and increase in Bcas1$^+$ cells (mean $\pm$ s.d., n = 6–9 mice).

(C) Quantification of cell marker immunofluorescence shows an increase in Bcas1$^+$ and CC1$^+$ area (mean $\pm$ s.d., n = 6 mice).

(D) Quantification of cell marker immunofluorescence shows a decrease in the number of GST-π$^+$ cells (mean $\pm$ s.d., n = 6–8 mice).

(E) Quantification of cell marker immunofluorescence shows a decrease in GST-π$^+$ area (mean $\pm$ s.d., n = 6–8 mice). These data, together with other findings, suggest that Ddx54 knockout primarily disables a very late stage of oligodendrocyte maturation when compensatory induction of oligodendrocyte differentiation may occur. For details, see discussion. Statistical analysis was performed using Student's t test. N.S., not significant.
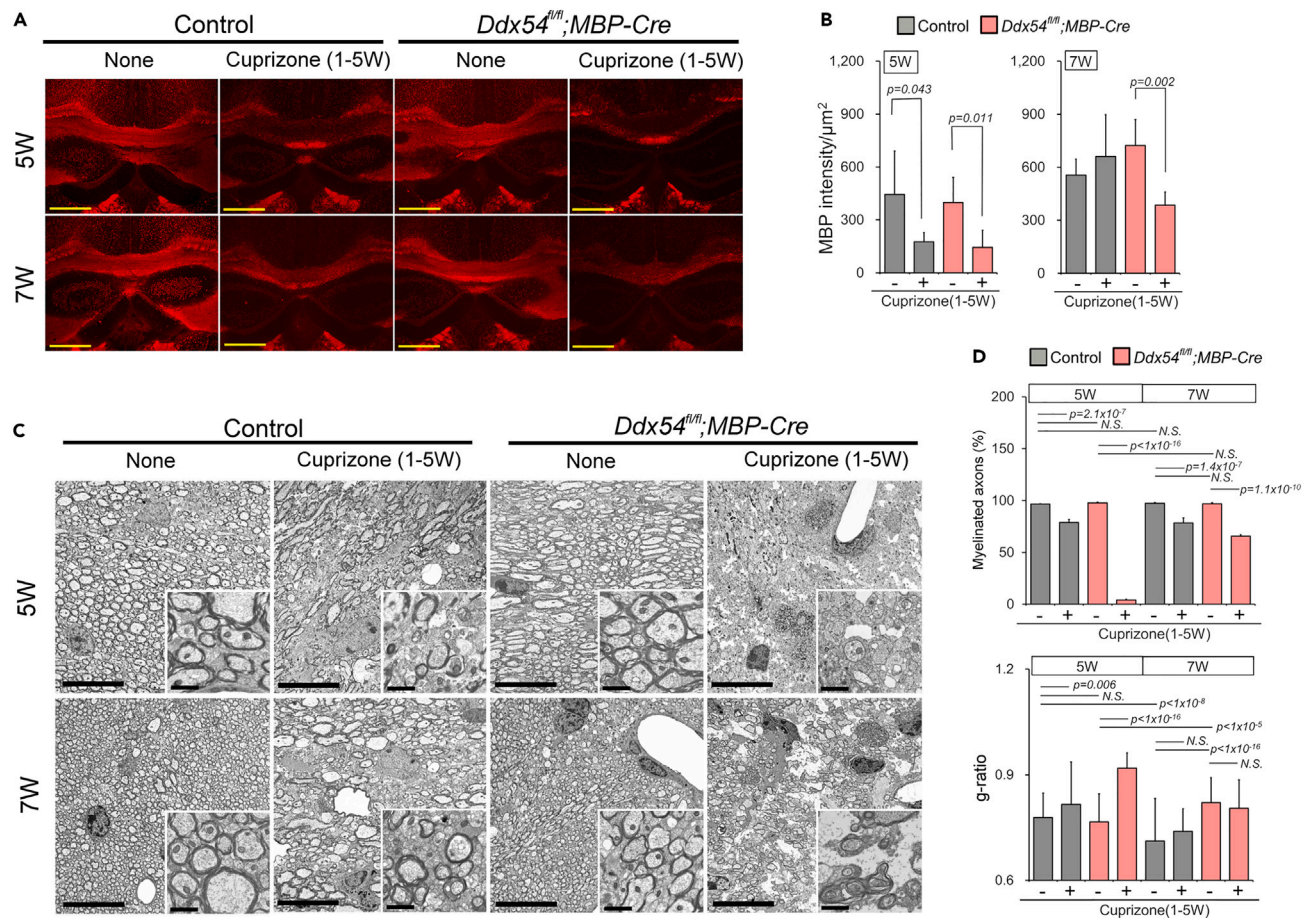
Figure 5. Ddx54 knockout induces remyelination failure in the cuprizone demyelination/remyelination model

(A) Immunohistochemical MBP staining of the forebrain of 5-week-old cuprizone-treated mice shows extensive depletion of MBP at the end of treatment (5W) in both Control and *Ddx54*$^{fl/fl}$;*MBP-Cre* mice. At 2 weeks after cuprizone removal (7W), control mice show full recovery in the amount of MBP, while recovery was incomplete in *Ddx54*$^{fl/fl}$;*MBP-Cre* mice. Scale bars represent 500 μm.

(B) Quantification of MBP immunofluorescence (n = 5 mice) in the CC.

(C) Electron microscopy of the CC of Control and *Ddx54*$^{fl/fl}$;*MBP-Cre* mice in the cuprizone model at 5W and 7W. *Ddx54*$^{fl/fl}$;*MBP-Cre* mice show almost complete depletion of myelinated axons at 5W. At 7W, tissue destruction progresses and many remyelinating axons breakdown despite the myelin sheath being reconstructed in some axons. Scale bars represent 10 μm (inlet: 1 μm).

(D) Upper panel: Number of myelinated axons (n = 3 fields counted from a set of littermate mice). Lower Panel: Average g-ratio (n = 114 axons counted from a set of littermate mice).

Data in (B and D) are represented as mean ± s.d. Statistical analysis methods were unpaired Student's *t* test for B and Bonferroni's multiple comparisons test for (D).

Ddx54$^{fl/fl}$;*MBP-Cre* mice exhibit impaired remyelination capacity

Abrupt breakdown of myelin after maturation implicates a critical role of Ddx54 in myelination in adulthood; i.e., such as in myelin repair, adaptive myelination, and/or myelin remodeling. To test this hypothesis, remyelination after cuprizone-induced demyelination in adult mice was evaluated. Nine-week old control and *Ddx54*$^{fl/fl}$;*MBP-Cre* mice, both show normal myelination, were treated with the neurotoxicant cuprizone in the diet for 5 weeks. Both strains exhibit demyelination by immunohistochemical MBP staining (Figures 5A and 5B) and electron microscopy (Figures 5C and 5D). Notably, almost complete demyelination is observed in "5W" *Ddx54*$^{fl/fl}$;*MBP-Cre* mice. Withdrawal of cuprizone induced spontaneous remyelination in both strains, however in *Ddx54*$^{fl/fl}$;*MBP-Cre* mice, tissue destruction continues to progress, with many axons exhibiting obvious breakdown of remyelination (Figure 5C, inlet), while some axons show apparently complete remyelination (Figures 5C and 5D). Analysis of oligodendrocyte differentiation markers of "7W" mice (Figures S8A–S8D) revealed, while the increase in Olig2$^+$ and Sox10$^+$ cells is modest (Figure S8B), the number and area of Bcas1$^+$ cells markedly increased in remyelinating brains after withdrawal of cuprizone
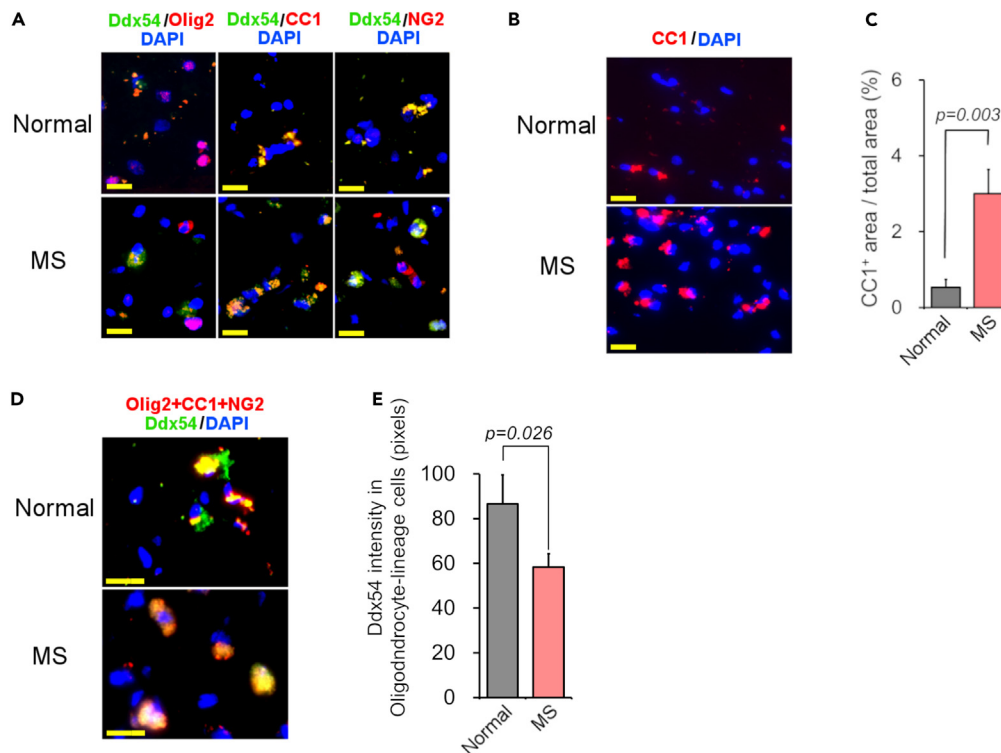
Figure 6. Oligodendrocytic Ddx54 decrease in multiple sclerosis patients

(A) Representative images of double immunostaining by Olig2, CC1 or NG2 and Ddx54. Scale bars represent 20 μm.

(B) Representative images of immunostaining by CC1. Scale bars represent 20 μm.

(C) Quantification of CC1$^+$ area in total area (mean ± s.d., n = 3 persons).

(D) Representative images of double immunostaining by Olig2+CC1+NG2 (3 antibody mix) and Ddx54. Scale bars represent 20 μm.

(E) Quantification of Ddx54 intensity in oligodendrocyte-lineage cells (Olig2$^+$ or CC1$^+$ or NG2$^+$ area) (mean ± s.d., n = 3 persons). Statistical analysis was performed using Student's t test.

both in *Ddx54$^{fl/fl}$;MBP-Cre* and control mice (Figure S8C). The number and/or area of NG2$^+$, CC1$^+$ and GST-π$^+$ cells also increased in both strains (Figure S8D). The increases in the number and/or area of NG2 and CC1 in *Ddx54$^{fl/fl}$;MBP-Cre* mice appears to be weaker than those of control mice, however, the difference did not attain statistical significance. However, the increases in GST-π immunosignals in *Ddx54$^{fl/fl}$;MBP-Cre* mice were clearly less than those in the control mice.

In vitro co-cultures of oligodendrocytes and neurons show that knockdown of Ddx54 by a lentiviral vector encoding shRNA to Ddx54, potently decreased myelination (Figures S9A–S9H).

Ddx54 expression in human corpus callosum

Immunohistochemistry of Ddx54 protein in the CC of MS patients is shown in Figure 6. Expression profile of Ddx54 protein is similar to that of mice (Figure 6A). Compared to normal controls, CC1$^+$ area increased (Figures 6B and 6C) and Ddx54 expression in oligodendrocyte-lineage cells decreased (Figures 6D and 6E) in MS patients. The results suggest that the maturation of oligodendrocyte-lineage cells, for presumably myelin repair, was enhanced with the decrease in Ddx54 in oligodendrocyte-lineage cells in MS patients.

DISCUSSION

In MS, impaired myelin sheath formation despite the presence of mature oligodendrocytes, as well as defective oligodendrocyte differentiation, loss of oligodendrocytes, and hostile environmental factors provided by microglia and astrocytes, contributes to (re)myelination failure.[23,24] Numerous strains of mutant,

transgenic and knockout mice in which genes involved in oligodendrocyte differentiation, myelination, and remyelination are dysregulated have been reported to show induction of CNS demyelination.[11,25] The shiverer mice carrying an autosomal recessive loss-of-function mutation in the MBP gene develop a shivering gait and tonic convulsions within a few weeks of birth with severe postnatal myelin malformation and usually die between 50 and 100 days after birth.[26] Although *Ddx54^{fl/fl};MBP-Cre* mice establish complete myelination until age 2 months and myelin breakdown begins at 4–5 months. This myelin breakdown occurs primarily from inside the axon and axonal swelling. Subsequent gliosis is associated with behavioral changes such as the development of tonic convulsions, ataxia, episodes of immobility and hiccup-like movement followed ultimately by death within age 7 months. These phenotypes are different from those of shiverer mice but, taken together with the abnormal behaviors shown in Figure 1, suggest dysregulation of motor control and posture reflexes. Indeed, such traits are common among various mouse strains with CNS demyelination.[27]

Disruption of the established myelin sheath after completion of postnatal myelination has rarely been reported. Artificial induction of myelin breakdown such as the use of agent-induced oligodendrocyte-specific toxicants (e.g., tumor necrosis factor[28] or diphtheria toxin[29]) have been employed, but it is difficult to investigate the etiology of human demyelinating disease using this approach. Most similar phenotypes to those described here have been described in CNPase knockout mice,[30] in which ataxia begins at age 4 months, followed by myelin disorder with axonal swellings noted at 7 months, and eventually gliosis. The mice died within 15 months (mostly within 7–11 months of age). CNPase localizes in the cytosol of oligodendrocytes and interacts with the cytoskeleton and plasma membrane providing an intracellular strut that counteracts membrane compaction by MBP and maintains the integrity of axon-glia interactions at nodes of Ranvier.[30,31] In CNPase knockout mice, axonal degeneration is observed since beginning in the very early postnatal period,[32] several months before the onset of behavioral changes and premature death. These findings suggest that loss of CNPase does not directly destroy myelin structure and that a slowly developing axonopathy must reach a threshold level before becoming clinically noticeable. On the other hand, axons of *Ddx54^{fl/fl};MBP-Cre* mice show no morphological aberration during postnatal neurodevelopment and breakdown of myelin occurs abruptly in adulthood, with shedding of myelinated axon-oligodendrocyte bundles giving rise to scattered holes in the apparently normal tissue. This suggests that a more rapid and direct disintegration of myelin sheath occurs in the established axon-oligodendrocyte complex in *Ddx54^{fl/fl};MBP-Cre* mice.

Vulnerability of myelinated axons and defective remyelination capacity shown in cuprizone experiments suggest that Ddx54 plays an important role in the maintenance of adult myelin and remyelination. The specific role of Ddx54 in adult myelin homeostasis is in contrast to that of another DEAD-box RNA helicase, Ddx20. With the same MBP-Cre system, Ddx20 knockout mice have been shown to have a decrease in the number of mature oligodendrocytes and expression of myelin related genes, as well as hypomyelination in the postnatal period with a lifespan of 2 months[33] By contrast, analysis of oligodendrocyte differentiation markers indicates that oligodendrocyte-lineage cells of *Ddx54^{fl/fl};MBP-Cre* mice can differentiate, at least until just before myelin sheath formation. In the present study, Bcas1 was either undetectable or detected only at trace amounts in the control and in *Ddx54^{fl/fl};MBP-Cre* mice at P10, 2 Mo and 4 Mo (cuprizone-untreated "7W" mice in the cuprizone experiment were 4 months of age). Only in 6.5 Mo *Ddx54^{fl/fl};MBP-Cre* mice and in the cuprizone-treated control and *Ddx54^{fl/fl};MBP-Cre* mice, was Bcas1 strongly induced. The Bcas1 immunosignal has been reported to be a useful marker for newly formed myelinated oligodendrocytes segregating from OPCs.[21] Thus, the present findings suggest that the decrease in Olig2 and increase of Bcas1 and CC1 reflect the onset of differentiation in pre-existing OPCs and immature oligodendrocytes for remyelination to compensate for myelin loss induced by Ddx54 knockout, rather than Ddx54 directly interfering with the differentiation process. Only the immunosignal corresponding to GST-π decreased. GST-π is a marker of mature, myelinating oligodendrocytes,[34] which is regulated downstream of MYRF1[35] and whose cytoplasmic form is known to partially exist in the myelin sheath.[36] The data suggest that Ddx54 is specifically involved in the final stage of oligodendrocyte differentiation and/or the process of myelination of axons. In our previous paper,[13] we demonstrated that a bolus injection of Ddx54 shRNA into the head of mice strongly prevented the penetration of MBP into the CC. In that experiment, virtually no MBP signal was detected in the CC. However, MBP was still present and found to accumulate in the subplate layer in front of the CC. Surprisingly, another myelin sheath protein, myelin-associated glycoprotein was found to enter the CC. Ddx54 may be required to transport MBP to the contact point between the oligodendrocyte process and neuronal axon.

DEAD-box proteins are ATP-dependent RNA helicases and play multiple cellular roles in processes such as synthesis, nuclear processing and export, translation, and the storage, splicing, and decay of RNAs, as well as ribonucleoprotein assembly.[37] Ddx54 has been reported to interact with estrogen receptors, CAR-binding protein and spliceosomal proteins regulating DNA damage repair, and plays an oncogenic role in several types of cancers.[38] We have shown that Ddx54 interacts with both mRNA and proteins of MBP isoforms, alter the nuclear translocation of exon 2-containing 21.5 kDa MBP, affects MBP promoter activity[12] and inhibits the contact of MBP-containing myelin and axons.[13] These findings suggest that Ddx54 plays a multifaceted critical roles in myelin biology through interaction with MBP mRNA and protein. Ddx54 is known to interact with 14-3-3 proteins[39] that are one of the most abundant proteins in the brain and has been detected in glial cells and cerebrospinal fluid of MS patients.[40] Furthermore, paralog analysis of 9338 individuals has identified DDX54 as a gene for which pathogenic variant alleles are involved in neurodevelopmental disorders.[41]

The data shown in Figure 6 suggests a possible involvement of Ddx54 in the pathogenesis of MS. Unfortunately, we could only obtain commercial MS specimens for which the number and information concerning patient and disease status were quite limited. Because demyelination and axon damage of $Ddx54^{fl/fl}$;MBP-Cre mice does not accompany peripheral lymphocyte infiltration, the mice are unsuitable as models of CNS inflammatory demyelinating diseases such as acute disseminated encephalomyelitis, neuromyelitis optica spectrum disorders and myelin oligodendrocyte glycoprotein antibody-associated disease, as well as relapsing-remitting MS and active secondary progressive MS. These disorders are generally characterized by peripheral inflammatory infiltrates consisting of lymphocytes and/or granulocytes.[42] However, in primary progressive MS and secondary progressive MS without clinical attack, active plaques are much less frequent. Spontaneous remyelination is incomplete or fails in secondary progressive MS despite the use of immunomodulation therapies, which are effective for relapsing-remitting MS.[43,44] This suggests that either an intrinsic mechanism or other unknown aspects of the lesion environment contribute to remyelination capacity. Thus, extensive studies involving collaboration with clinical researchers of MS will be needed to firmly establish whether Ddx54 plays a role in the pathogenesis of MS.

Elucidation of the involvement of Ddx54 in remyelination might contribute to the understanding of the mechanisms of leukodystrophies, a group of progressive, neurogenetic disease affecting white matter pathology with abnormalities in myelin sheath and significant axonal pathology.[45] Leukodystrophies are increasingly recognized as a disease group in which glial cells are the primary players and the list of diseases are continuously growing, in parallel with advances in laboratory models. In addition, other CNS pathologies classically considered strictly neurodegenerative, such as amyotrophic lateral sclerosis,[46] schizophrenia,[47] Alzheimer's disease,[48] Parkinson's disease,[49] the spectrum of autistic dysfunctions,[50] and age-related brain function decline,[51] are characterized by nerve demyelination at an early stage of the disease. $Ddx54^{fl/fl}$;MBP-Cre mice thus provide a new model for investigating the mechanism of myelination/remyelination, especially in the adult (e.g., myelin repair, adaptive myelination, and/or myelin remodeling), which will lead to the development of pharmacological therapies for various CNS diseases. Indeed, because the efficiency of gene deletion is in principle leaky in the Cre-loxP system, the present model can be used to investigate potentially beneficial agents, as exemplified by Figure S9I, showing a life prolongation effect of a certain herbal medicine in $Ddx54^{fl/fl}$;MBP-Cre mice.

Limitations of the study

In the present model, (1) severe demyelination occurs in adults but not in early postnatal myelination, (2) disintegration of myelin sheath formation, rather than hypomyelination and/or suppression of oligodendrocyte differentiation, induces axonal breakdown, and (3) infiltration of peripheral lymphocytes was not observed. The unique feature of this model may contribute to the clarification of aspects of human demyelinating diseases that have rarely been addressed. Why does the onset of MS mostly occur in adulthood? Why does neurodegeneration accumulate in MS patients despite the success of immunomodulating therapies to reduce or even halt disease progression? What is the mechanism of myelin breakdown that does not involve an inflammatory response as frequently observed in various CNS diseases as well as progressive MS? Unfortunately, in the present study, we could not investigate the molecular mechanism of demyelination caused by Ddx54 knockdown. Therefore, it is unclear which disease(s) these Ddx54 knockdown mice best model. In the present study, we could only use commercial MS specimens for which the number and information concerning patient and disease status were quite limited. Further extensive studies in collaboration with clinical researchers of MS and other CNS diseases will be required. Moreover, some of the

experiments in this study involved relatively small numbers of animals. Consequently, rigorous analysis of molecular events was not possible. Nonetheless, the results obtained in the present study suggest larger scale clinical and basic studies on Ddx54 are warranted.

STAR★METHODS

Detailed methods are provided in the online version of this paper and include the following:

- KEY RESOURCES TABLE
- RESOURCE AVAILABILITY
    - Lead contact
    - Materials availability
    - Data and code availability
- EXPERIMENTAL MODEL AND SUBJECT DETAILS
    - Animals
    - Cells and viruses
    - Ethical statement
    - Generation and propagation of genetically modified mice
    - Genotyping primer information
- METHOD DETAILS
    - Voluntary activity
    - Rotarod testing
    - Y maze test
    - Macroscopic observation, histopathology, and Luxol fast blue staining
    - Tissue lysis and immunoblotting
    - Immunohistochemistry
    - Electron microscopy
    - TUNEL assay
    - Cuprizone experiment
    - Oligodendrocyte-neuronal co-cultures
    - Preparation of plasmids containing short hairpin RNAs (shRNAs)
    - Production of retroviruses and retrovirus-mediated DNA transfection
    - Effect of an herbal medicine on $Ddx54^{fl/fl}$;MBP-Cre mice
- QUANTIFICATION AND STATISTICAL ANALYSIS

AUTHOR CONTRIBUTIONS

Conceptualization: H.A., J.Y., and M.Y. Methodology: J.Y., K.M., and K.O. Investigation: H.O., S.I., N.Y., C.S., M.Y., and Y.M. Validation: M.Y., H.O., Y.M., J.Y., C.S., and H.A. Data Curation and Formal Analysis: H.O., S.I. M.Y., Y.M., and T.T. Writing – Original Draft: M.Y. Writing – Review and Editing: M.Y., Y.M., J.Y., and H.A. Visualization: H.O., Y.M., and M.Y. Supervision: H.A., J.Y., and M.Y. Project administration: H.A., J.Y., and M.Y. Funding acquisition: J.Y. and M.Y.

DECLARATION OF INTERESTS

M.Y., H.O., K.O., S.I., and K.M., are employees of Tsumura & Co.

J.Y. received research grants for the present study from Takeda Science Foundation and Tsumura & Co.

The other authors declare no competing interests.

INCLUSION AND OF DIVERSITY

We support inclusive, diverse, and equitable conduct of research.

REFERENCES

1. Kutzelnigg, A., and Lassmann, H. (2014). Pathology of multiple sclerosis and related inflammatory demyelinating diseases. Handb. Clin. Neurol. 122, 15–58. https://doi.org/10.1016/B978-0-444-52001-2.00002-9.

2. Faissner, S., Plemel, J.R., Gold, R., and Yong, V.W. (2019). Progressive multiple sclerosis: From pathophysiology to therapeutic strategies. Nat. Rev. Drug Discov. 18, 905–922. https://doi.org/10.1038/s41573-019-0035-2.

3. Macaron, G., and Ontaneda, D. (2019). Diagnosis and management of progressive multiple sclerosis. Biomedicines 7, 56. https://doi.org/10.3390/biomedicines7030056.

4. Macchi, M., Magalon, K., Zimmer, C., Peeva, E., El Waly, B., Brousse, B., Jaekel, S., Grobe, K., Kiefer, F., Williams, A., et al. (2020). Mature oligodendrocytes bordering lesions limit demyelination and favor myelin repair via heparan sulfate production. Elife 9, e51735. https://doi.org/10.7554/eLife.51735.

5. Marques, S., Zeisel, A., Codeluppi, S., van Bruggen, D., Mendanha Falcão, A., Xiao, L., Li, H., Häring, M., Hochgerner, H., Romanov, R.A., et al. (2016). Oligodendrocyte heterogeneity in the mouse juvenile and adult central nervous system. Science 352, 1326–1329. https://doi.org/10.1126/science.aaf6463.

6. Tripathi, R.B., Jackiewicz, M., McKenzie, I.A., Kougioumtzidou, E., Grist, M., and Richardson, W.D. (2017). Remarkable stability of myelinating oligodendrocytes in mice. Cell Rep. 21, 316–323. https://doi.org/10.1016/j.celrep.2017.09.050.

7. van Bruggen, D., Agirre, E., and Castelo-Branco, G. (2017). Single-cell transcriptomic analysis of oligodendrocyte lineage cells. Curr. Opin. Neurobiol. 47, 168–175. https://doi.org/10.1016/j.conb.2017.10.005.

8. Jäkel, S., Agirre, E., Mendanha Falcão, A., van Bruggen, D., Lee, K.W., Knuesel, I., Malhotra, D., Ffrench-Constant, C., Williams, A., and Castelo-Branco, G. (2019). Altered human oligodendrocyte heterogeneity in multiple sclerosis. Nature 566, 543–547. https://doi.org/10.1038/s41586-019-0903-2.

9. Yeung, M.S.Y., Djelloul, M., Steiner, E., Bernard, S., Salehpour, M., Possnert, G., Brundin, L., and Frisén, J. (2019). Dynamics of oligodendrocyte generation in multiple sclerosis. Nature 566, 538–542. https://doi.org/10.1038/s41586-018-0842-3.

10. Spaas, J., van Veggel, L., Schepers, M., Tiane, A., van Horssen, J., Wilson, D.M., 3rd, Moya, P.R., Piccart, E., Hellings, N., Eijnde, B.O., et al. (2021). Oxidative stress and impaired oligodendrocyte precursor cell differentiation in neurological disorders. Cell. Mol. Life Sci. 78, 4615–4637. https://doi.org/10.1007/s00018-021-03802-0.

11. Tognatta, R., and Miller, R.H. (2016). Contribution of the oligodendrocyte lineage to CNS repair and neurodegenerative pathologies. Neuropharmacology 110, 539–547. https://doi.org/10.1016/j.neuropharm.2016.04.026.

12. Ueki, T., Tsuruo, Y., Yamamoto, Y., Yoshimura, K., Takanaga, H., Seiwa, C., Motojima, K., Asou, H., and Yamamoto, M. (2012). A new monoclonal antibody, 4F2, specific for the oligodendroglial cell lineage, recognizes ATP-dependent RNA helicase Ddx54: possible association with myelin basic protein. J. Neurosci. Res. 90, 48–59. https://doi.org/10.1002/jnr.22736.

13. Zhan, R., Yamamoto, M., Ueki, T., Yoshioka, N., Tanaka, K., Morisaki, H., Seiwa, C., Yamamoto, Y., Kawano, H., Tsuruo, Y., et al. (2013). A DEAD-box RNA helicase Ddx54 protein in oligodendrocytes is indispensable for myelination in the central nervous system. J. Neurosci. Res. 91, 335–348. https://doi.org/10.1002/jnr.23162.

14. Feldman, M.L., and Peters, A. (1998). Ballooning of myelin sheaths in normally aged macaques. J. Neurocytol. 27, 605–614. https://doi.org/10.1023/a:1006926428699.

15. Duncan, I.D., and Radcliff, A.B. (2016). Inherited and acquired disorders of myelin: The underlying myelin pathology. Exp. Neurol. 283 (Pt B), 452–475. https://doi.org/10.1016/j.expneurol.2016.04.002.

16. Kirk, J. (1979). The fine structure of the CNS in multiple sclerosis. II. Vesilcular demyelination in an acute case. Neuropathol. Appl. Neurobiol. 5, 289–294. https://doi.org/10.1111/j.1365-2990.1979.tb00627.x.

17. Périer, O., and Grégoire, A. (1965). Electron microscopic features of multiple sclerosis lesions. Brain 88, 937–952. https://doi.org/10.1093/brain/88.5.937.

18. Rodriguez, M., Scheithauer, B.W., Forbes, G., and Kelly, P.J. (1993). Oligodendrocyte injury is an early event in lesions of multiple sclerosis. Mayo Clin. Proc. 68, 627–636. https://doi.org/10.1016/S0025-6196(12)60597-7.

19. Rodriguez, M., and Scheithauer, B. (1994). Ultrastructure of multiple sclerosis. Ultrastruct. Pathol. 18, 3–13. https://doi.org/10.3109/01913129409016267.

20. Suzuki, K., Andrews, J.M., Waltz, J.M., and Terry, R.D. (1969). Ultrastructural studies of multiple sclerosis. Lab. Invest. 20, 444–454.

21. Fard, M.K., van der Meer, F., Sánchez, P., Cantuti-Castelvetri, L., Mandad, S., Jäkel, S., Fornasiero, E.F., Schmitt, S., Ehrlich, M., Starost, L., et al. (2017). BCAS1 expression defines a population of early myelinating oligodendrocytes in multiple sclerosis lesions. Sci. Transl. Med. 9, eaam7816. https://doi.org/10.1126/scitranslmed.aam7816.

22. Li, W., and Teng, J. (2023). circCELF1 Induces the apoptosis and autophagy of astrocytes in ischemic stroke via upregulating NFAT5. Cerebrovasc. Dis. 52, 306–317. https://doi.org/10.1159/000526359.

23. Heß, K., Starost, L., Kieran, N.W., Thomas, C., Vincenten, M.C.J., Antel, J., Martino, G., Huitinga, I., Healy, L., and Kuhlmann, T. (2020). Lesion stage-dependent causes for impaired remyelination in MS. Acta Neuropathol. 140, 359–375. https://doi.org/10.1007/s00401-020-02189-9.

24. Stadelmann, C., Timmler, S., Barrantes-Freer, A., and Simons, M. (2019). Myelin in the central nervous system: Structure, function, and pathology. Physiol. Rev. 99, 1381–1431. https://doi.org/10.1152/physrev.00031.2018.

25. Chamberlain, K.A., Nanescu, S.E., Psachoulia, K., and Huang, J.K. (2016). Oligodendrocyte regeneration: Its significance in myelin replacement and neuroprotection in multiple sclerosis. Neuropharmacology 110, 633–643. https://doi.org/10.1016/j.neuropharm.2015.10.010.

26. Readhead, C., and Hood, L. (1990). The dysmyelinating mouse mutations shiverer (shi) and myelin deficient (shimld). Behav. Genet. 20, 213–234. https://doi.org/10.1007/BF01067791.

27. Nave, K.A. (1994). Neurological mouse mutants and the genes of myelin. J. Neurosci. Res. 38, 607–612. https://doi.org/10.1002/jnr.490380602.

28. Akassoglou, K., Bauer, J., Kassiotis, G., Pasparakis, M., Lassmann, H., Kollias, G., and Probert, L. (1998). Oligodendrocyte apoptosis and primary demyelination induced by local TNF/p55TNF receptor signaling in the central nervous system of transgenic mice: Models for multiple sclerosis with primary oligodendrogliopathy. Am. J.

Pathol. *153*, 801–813. https://doi.org/10.1016/S0002-9440(10)65622-2.

29. Traka, M., Podojil, J.R., McCarthy, D.P., Miller, S.D., and Popko, B. (2016). Oligodendrocyte death results in immune-mediated CNS demyelination. Nat. Neurosci. *19*, 65–74. https://doi.org/10.1038/nn.4193.

30. Lappe-Siefke, C., Goebbels, S., Gravel, M., Nicksch, E., Lee, J., Braun, P.E., Griffiths, I.R., and Nave, K.A. (2003). Disruption of Cnp1 uncouples oligodendroglial functions in axonal support and myelination. Nat. Genet. *33*, 366–374. https://doi.org/10.1038/ng1095.

31. Rasband, M.N., Tayler, J., Kaga, Y., Yang, Y., Lappe-Siefke, C., Nave, K.A., and Bansal, R. (2005). CNP is required for maintenance of axon-glia interactions at nodes of Ranvier in the CNS. Glia *50*, 86–90. https://doi.org/10.1002/glia.20165.

32. Edgar, J.M., McLaughlin, M., Werner, H.B., McCulloch, M.C., Barrie, J.A., Brown, A., Faichney, A.B., Snaidero, N., Nave, K.A., and Griffiths, I.R. (2009). Early ultrastructural defects of axons and axon-glia junctions in mice lacking expression of Cnp1. Glia *57*, 1815–1824. https://doi.org/10.1002/glia.20893.

33. Simankova, A., Bizen, N., Saitoh, S., Shibata, S., Ohno, N., Abe, M., Sakimura, K., and Takebayashi, H. (2021). Ddx20, DEAD box helicase 20, is essential for the differentiation of oligodendrocyte and maintenance of myelin gene expression. Glia *69*, 2559–2574. https://doi.org/10.1002/glia.24058.

34. Tansey, F.A., and Cammer, W. (1991). A pi form of glutathione-S-transferase is a myelin- and oligodendrocyte-associated enzyme in mouse brain. J. Neurochem. *57*, 95–102. https://doi.org/10.1111/j.1471-4159.1991.tb02104.x.

35. Duncan, G.J., Plemel, J.R., Assinck, P., Manesh, S.B., Muir, F.G.W., Hirata, R., Berson, M., Liu, J., Wegner, M., Emery, B., et al. (2017). Myelin regulatory factor drives remyelination in multiple sclerosis. Acta Neuropathol. *134*, 403–422. https://doi.org/10.1007/s00401-017-1741-7.

36. Tamura, Y., Kataoka, Y., Cui, Y., Takamori, Y., Watanabe, Y., and Yamada, H. (2007). Intracellular translocation of glutathione S-transferase pi during oligodendrocyte differentiation in adult rat cerebral cortex in vivo. Neuroscience *148*, 535–540. https://doi.org/10.1016/j.neuroscience.2007.06.026.

37. Putnam, A.A., and Jankowsky, E. (2013). DEAD-box helicases as integrators of RNA, nucleotide and protein binding. Biochim. Biophys. Acta *1829*, 884–893. https://doi.org/10.1016/j.bbagrm.2013.02.002.

38. Yu, Y., Wang, J.L., Meng, L.L., Hu, C.T., Yan, Z.W., He, Z.P., Shi, X.Q., Fu, G.H., and Zu, L.D. (2021). DDX54 plays a cancerous role through activating p65 and AKT signaling pathway in colorectal cancer. Front. Oncol. *11*, 650360. https://doi.org/10.3389/fonc.2021.650360.

39. Satoh, J.i., Nanri, Y., and Yamamura, T. (2006). Rapid identification of 14-3-3-binding proteins by protein microarray analysis. J. Neurosci. Methods *152*, 278–288. https://doi.org/10.1016/j.jneumeth.2005.09.015.

40. Kawamoto, Y., Akiguchi, I., Kovács, G.G., Flicker, H., and Budka, H. (2004). Increased 14-3-3 immunoreactivity in glial elements in patients with multiple sclerosis. Acta Neuropathol. *107*, 137–143. https://doi.org/10.1007/s00401-003-0785-z.

41. Paine, I., Posey, J.E., Grochowski, C.M., Jhangiani, S.N., Rosenheck, S., Kleyner, R., Marmorale, T., Yoon, M., Wang, K., Robison, R., et al. (2019). Paralog studies augment gene discovery: DDX and DHX genes. Am. J. Hum. Genet. *105*, 302–316. https://doi.org/10.1016/j.ajhg.2019.06.001.

42. Höftberger, R., and Lassmann, H. (2017). Inflammatory demyelinating diseases of the central nervous system. Handb. Clin. Neurol. *145*, 263–283. https://doi.org/10.1016/B978-0-12-802395-2.00019-5.

43. Dighriri, I.M., Aldalbahi, A.A., Albeladi, F., Tahiri, A.A., Kinani, E.M., Almohsen, R.A., Alamoudi, N.H., Alanazi, A.A., Alkhamshi, S.J., Althomali, N.A., et al. (2023). An overview of the history, pathophysiology, and pharmacological interventions of multiple sclerosis. Cureus *15*, e33242. https://doi.org/10.7759/cureus.33242.

44. Dimitriou, N.G., Meuth, S.G., Martinez-Lapiscina, E.H., Albrecht, P., and Menge, T. (2023). Treatment of patients with multiple sclerosis transitioning between relapsing and progressive disease. CNS Drugs *37*, 69–92. https://doi.org/10.1007/s40263-022-00977-3.

45. Garcia, L.M., Hacker, J.L., Sase, S., Adang, L., and Almad, A. (2020). Glial cells in the driver seat of leukodystrophy pathogenesis. Neurobiol. Dis. *146*, 105087. https://doi.org/10.1016/j.nbd.2020.105087.

46. Zhou, T., Ahmad, T.K., Gozda, K., Truong, J., Kong, J., and Namaka, M. (2017). Implications of white matter damage in amyotrophic lateral sclerosis (Review). Mol. Med. Rep. *16*, 4379–4392. https://doi.org/10.3892/mmr.2017.7186.

47. Tkachev, D., Mimmack, M.L., Ryan, M.M., Wayland, M., Freeman, T., Jones, P.B., Starkey, M., Webster, M.J., Yolken, R.H., and Bahn, S. (2003). Oligodendrocyte dysfunction in schizophrenia and bipolar disorder. Lancet *362*, 798–805. https://doi.org/10.1016/S0140-6736(03)14289-4.

48. Nasrabady, S.E., Rizvi, B., Goldman, J.E., and Brickman, A.M. (2018). White matter changes in Alzheimer's disease: A focus on myelin and oligodendrocytes. Acta Neuropathol. Commun. *6*, 22. https://doi.org/10.1186/s40478-018-0515-3.

49. Xie, S., Yang, J., Huang, S., Fan, Y., Xu, T., He, J., Guo, J., Ji, X., Wang, Z., Li, P., et al. (2022). Disrupted myelination network in the cingulate cortex of Parkinson's disease. IET Syst. Biol. *16*, 98–119. https://doi.org/10.1049/syb2.12043.

50. Rahi, S., and Mehan, S. (2022). Understanding abnormal SMO-SHH aignaling in autism spectrum disorder: Potential drug target and therapeutic goals. Cell. Mol. Neurobiol. *42*, 931–953. https://doi.org/10.1007/s10571-020-01010-1.

51. Zhang, X., Huang, N., Xiao, L., Wang, F., and Li, T. (2021). Replenishing the aged rrains: Targeting oligodendrocytes and myelination? Front. Aging Neurosci. *13*, 760200. https://doi.org/10.3389/fnagi.2021.760200.

52. Friedel, R.H., Wurst, W., Wefers, B., and Kühn, R. (2011). Generating conditional knockout mice. Methods Mol. Biol. *693*, 205–231. https://doi.org/10.1007/978-1-60761-974-1_12.

53. Niwa-Kawakita, M., Abramowski, V., Kalamarides, M., Thomas, G., and Giovannini, M. (2000). Targeted expression of Cre recombinase to myelinating cells of the central nervous system in transgenic mice. Genesis *26*, 127–129. https://doi.org/10.1002/(SICI)1526-968X(200002)26:2<127::AID-GENE8>3.0.CO;2-H.

54. Farhadi, H.F., Lepage, P., Forghani, R., Friedman, H.C.H., Orfali, W., Jasmin, L., Miller, W., Hudson, T.J., and Peterson, A.C. (2003). A combinatorial network of evolutionarily conserved myelin basic protein regulatory sequences confers distinct glial-specific phenotypes. J. Neurosci. *23*, 10214–10223. https://doi.org/10.1523/JNEUROSCI.23-32-10214.2003.

55. Miyamoto, Y., Torii, T., Terao, M., Takada, S., Tanoue, A., Katoh, H., and Yamauchi, J. (2021). Rnd2 differentially regulates oligodendrocyte myelination at different developmental periods. Mol. Biol. Cell *32*, 769–787. https://doi.org/10.1091/mbc.E20-05-0332.

56. Kraeuter, A.K., Guest, P.C., and Sarnyai, Z. (2019). The Y-Maze for assessment of spatial working and reference memory in mice. Methods Mol. Biol. *1916*, 105–111. https://doi.org/10.1007/978-1-4939-8994-2_10.

57. Vega-Riquer, J.M., Mendez-Victoriano, G., Morales-Luckie, R.A., and Gonzalez-Perez, O. (2019). Five decades of cuprizone, an updated model to replicate demyelinating diseases. Curr. Neuropharmacol. *17*, 129–141. https://doi.org/10.2174/1570159X15666170717120343.

STAR★METHODS

KEY RESOURCES TABLE

REAGENT or RESOURCE	SOURCE	IDENTIFIER
Antibodies		
chicken polyclonal anti-MBP	EnCor Biotechnology Inc.	Cat# CPCA-MBP; RRID: AB_2572352
mouse monoclonal anti-MBP	Covance	Cat# SMI-94R-500; RRID: AB_510040
rabbit polyclonal anti-GFAP	Proteintech Group Inc.	Cat# 23935-1-AP; RRID: AB_2879367
rabbit polyclonal anti-GFAP	Covance	Cat# PRB-571C-100; RRID: AB_291696
mouse monoclonal anti-GFAP	Merck Millipore	Cat# 05-675; RRID: AB_309896
mouse monoclonal anti-Iba1	Merck Millipore	Cat# MABN92; RRID: AB_10917271
mouse monoclonal anti-NeuN	Merck Millipore	Cat# MAB377; RRID: AB_2298772
rabbit monoclonal anti-NeuN	Abcam	Cat# ab177487; RRID: AB_2532109
rabbit polyclonal anti-200 kDa neurofilament protein	Merck Millipore	#N4142
rabbit polyclonal anti-NG2	Merck Millipore	Cat# AB5320; RRID: AB_91789
mouse monoclonal anti-tubulin β3 (TuJ1)	BioLegend	Cat# 801202; RRID: AB_10063408
mouse monoclonal anti-2′, 3′-cyclicnucleotide 3′-phosphodiestrase	Sigma-Aldrich	Cat# C5922; RRID: AB_476854
mouse monoclonal anti-actin	Fujifilm Wako Pure Chemical Co.	#281-98721
goat polyclonal anti-Ddx54	Santa Cruz Biotechnology	Cat# sc-132652; RRID: AB_2091107
mouse monoclonal anti-Ddx54	in house	Ueki et al.[12]
rabbit monoclonal anti-Olig2	Abcam	Cat# ab109186; RRID: AB_10861310
mouse monoclonal anti-adenomatus polyposis coli (CC1)	GenTex, Inc.	clone CC1
rabbit monoclonal anti-S100A10	Abcam	Cat# ab76472; RRID: AB_1524359
goat polyclonal anti-C3d	R&D Systems	Cat# AF2655; RRID: AB_2066622
rabbit polyclonal anti-iNOS	Novus Biochemicals, LLC	Cat# NBP1-50606; RRID: AB_10012794
rabbit polyclonal anti-Arg1	Bioss Antibodies	bs-8585R
rabbit monoclonal anti-Sox10	Abcam	Cat# ab227680; RRID: AB_2927464
rabbit polyclonal MYRF/C11orf9 Polyclonal Antibody	Funakoshi	bs-11191R
rabbit polyclonal GPR17 Polyclonal Antibody	Funakoshi	bs-12022RR
rabbit polyclonal anti-GST-π	MBL	Cat# 312; RRID: AB_591792
rabbit polyclonal anti-Bcas1	Bioss	bs-11462R
Biological samples		
Human corpus callosum frozen tissue (Normal adult)	BioChain	T1234045
Human corpus callosum Frozen tissue (Multiple sclerosis adult)	BioChain	T12346045Msc
Chemicals, peptides, and recombinant proteins		
cuprizone	Kanto Chemical, Tokyo, Japan	04198-30
Critical commercial assays		
TACS·XL-Blue Label *in Situ* Apoptosis Detection kit	Trevigen (R&D Systems, Inc.)	RSD 4828-30-BK

(Continued on next page)

Continued

REAGENT or RESOURCE	SOURCE	IDENTIFIER
CalPhos Mammalian Transfection kit	Takara Bio, Shiga, Japan	631312
Takara Bio retroviral production kit	Takara Bio, Shiga, Japan	6160
Experimental models: Organisms/strains		
MBP promoter– Cre recombinase transgenic mice	Riken BioResource Center (Ibaraki, Japan)	RBRC No. 01461
C57BL/6 mice	Jackson Laboratory Japan, Inc (Yokohama)	RRID:IMSR_JAX:000664
Recombinant DNA		
The retrovirus vector, pSINmU6	Takara Bio, Shiga, Japan	3662
Oligonucleotides		
Usage	Sequence	Detail
The chimera mice and F1 mice (Detection of 5′ homologous recombination) **F:**	CTCGAGTTTACGCAGCCAATAGAA	Genome, on the outside of 5′HR
The chimera mice and F1 mice (Detection of 5′ homologous recombination) **R:**	GGATAGGTCACGTTGGTGTAGAT	lacZ sequence
The chimera mice and F1 mice (Detection of 3′ homologous recombination) **F:**	CTTCCTCGTGCTTTACGGTATC	Neomycin resistance sequence
The chimera mice and F1 mice (Detection of 3′ homologous recombination) **R:**	TGTTCAAATAGGATGTACCCAGAG	Genome, on the outside of 3′ HR
The chimera mice and F1 mice (loxP seq detection) **F:**	ACATCAGAAGACACTGGTGAACTG	Genome, on the Exon
The chimera mice and F1 mice (loxP seq detection) **R:**	CTTTATACTTAGGTGTCAGGCATGG	loxP seq
Neo or/and FLP removal (Detection of Neo removed Targeted allele) **F:**	GATGAGGCTTTCGTTGTATAGGATA	Genome, on the 5′HR
Neo or/and FLP removal (Detection of Neo removed Targeted allele) **R:**	AGAAATGCTTACTGTGAGACACCTG	Genome, on the Exon
Neo or/and FLP removal (Neo Seq Detection) **F:**	GAACAAGATGGATTGCACGCAGGTTCTCCG	Neomycin resistance sequence
Neo or/and FLP removal (Neo Seq Detection) **R:**	GTAGCCAACGCTATGTCCTGATAG	Neomycin resistance sequence
Neo or/and FLP removal (FLP Seq detection) **F:**	TAGTTTGCAATTACAGTTCGAATCA	FLP sequence
Neo or/and FLP removal (FLP Seq detection) **R:**	AGCCTTGTTGTACGATCTGACTAAG	FLP sequence
Homo (loxP/loxP) mice (Floxed allele detection) **F:**	GATGAGGCTTTCGTTGTATAGGATA	FLP Genome, on the 5′HR
Homo (loxP/loxP) mice (Floxed allele detection) **R:**	AGAAATGCTTACTGTGAGACACCTG	Genome, on the Exon
FC and FFC mice (MBP-Cre cassette detection) **F:**	CAGGGGAGGCAGATGCGATCC	MBP Promoter seq
FC and FFC mice (MBP-Cre cassette detection) **R:**	CTAATCGCCATCTTCCAGCAGG	Cre Seq
The chimera mice and F1 mice (Detection of 3′ homologous recombination) **F:**	CTTCCTCGTGCTTTACGGTATC	Neomycin resistance sequence
The chimera mice and F1 mice (Detection of 3′ homologous recombination) **R:**	TGTTCAAATAGGATGTACCCAGAG	Genome, on the outside of 3′ HR
Ddx54#1 shRNA	GATCCGGTGCCAACACCCATCCAGCTGTGAAGCCACAGATGGGCTGGATGGGTGTTGGCACCTTTTTTACGCGTAT	sense
Ddx54#1 shRNA	CGATACGCGTAAAAAAGGTGCCAACACCCATCCAGCCCATCTGTGGCTTCACAGCTGGATGGGTGTTGGCACCG	antisense
Ddx54#2 shRNA	GATCCGACTGCCTTGATCCTGGGTCTGTGAAGCCACAGATGGGACCCAGGATCAAGGCAGTCTTTTTTACGCGTAT	sense

Continued

REAGENT or RESOURCE	SOURCE	IDENTIFIER
Ddx54#2 shRNA	CGATACGCGTAAAAAAGGTGCCAACAC CCATCCAGCCCATCTGTGGCTTCACAG CTGGATGGGTGTTGGCACCG	antisense
The control Photinus pyralis luciferase shRNA	GATCCGGCCATTCTATCCTCTAGACT GTGAAGCCACAGATGGGTCTAGAGG ATAGAATGGCCTTTTTTACGCGTAT	sense
The control Photinus pyralis luciferase shRNA	CGATACGCGTAAAAAAGGCCATTCTAT CCTCTAGACCCATCTGTGGCTTCACAG TCTAGAGGATAGAATGGCCG	antisense
Software and algorithms		
R ver. 2.8.1	R core team	https://www.R-project.org/
EZR (a graphical user interface for R)	Saitama Medical Center, Jichi Medical University	https://www.jichi.ac.jp/saitama-sct/ SaitamaHP.files/statmedEN.html
Prism ver.9.0	GraphPad	https://www.graphpad.com/
Microsoft Office Home	Microsoft Corporation	https://www.microsoft.com/microsoft-365
Image Analyzer BZ-H3A	KEYENCE CORPORATION	https://www.keyence.co.jp/products/ microscope/fluorescence-microscope/ bz-x700/models/bz-h3a/

RESOURCE AVAILABILITY

Lead contact

Further information and requests for resources should be directed to and will be fulfilled by the lead contact, Masahiro Yamamoto (hirokoma@h.email.ne.jp).

Materials availability

Specific requests about *Ddx54fl/fl;MBP-Cre* mice should be directed to Hiroaki Oizumi (ooizumi_hiroaki@ mail.tsumura.co.jp) or Junji Yamauchi (yamauchi@toyaku.ac.jp).

Data and code availability

- All data reported in this paper will be shared by the lead contact upon request.
- This paper does not report original code.
- Any additional information required to re-analyze the data reported in this paper is available from the lead contact upon request.

EXPERIMENTAL MODEL AND SUBJECT DETAILS

Animals

Naïve mice and rats were purchased from The Jackson Laboratory Japan (Yokohama, Japan). All experiments were performed using male animals.

Cells and viruses

G3Thi cells and viral vectors pVSVG and pGP were provided with the Takara Bio retroviral production kit (Takara Bio, Shiga, Japan).

Ethical statement

Generation and maintenance of genetically modified/unmodified mice and animal experiments using mice and rats were performed in accordance with a protocol approved by Unitech Animal Experiment Committee, Unitech Gene Modification Experiment Safety Committee, the Laboratory Animal Committee of

Tsumura & Co. and by the Japanese National Research Institute for Child Health and Development Animal Care Committee.

Generation and propagation of genetically modified mice

Mice in which the Ddx54 gene flanked by loxP sites (loxP/loxP) (FF) were generated by Unitech Co., Ltd. (Chiba, Japan) according to the routine method.[52] C57BL/6-background *Ddx54*^{fl/fl}*;MBP-Cre* mice were generated by interbreeding FF mice with MBPCre-9 mice,[53] propagated by Unitech and distributed to Tsumura & Co. and the Japanese National Research Institute for Child Health and Development by Unitech. FF mice were used as control mice. The activity of this promoter has been reported to be highly specific to OPCs and oligodendrocytes,[5,53,54] which we have confirmed in the previous study.[55] The animals were housed individually under controlled conditions of temperature (23 ± 2°C), humidity (55 ± 10%), and lighting (12-h light/dark cycle) and provided with food and water *ad libitum* under specific pathogen-free conditions. Mice were allocated cages/groups for experiments by animal technicians independently from the researchers.

Genotyping primer information

Mice PCR genotyping was performed using oligonucleotide primer sets as described in key resources table. Primer sets No. 1 and 2 amplify the a PCR product in the targeted allele of 7807 bp and 6935 bp, respectively. Primer set No.3 amplifies a 183 bp product in WT and a 154 bp product in the targeted allele. Primer set No. 4 amplifies a 357 bp product in WT and a 7423 bp product in the targeted allele with Neo, and a 519 bp product in the targeted allele without Neo. The Neo sequence itself was checked using primer set No. 5, which generates a 668 bp product, and FLP was checked by set No. 6, which generates a 496 bp product. Primer set No. 7 generates a 357 bp product in WT, and a 519 bp product in floxed alleles, respectively. Primer set No. 8 was used to detect the MBP-Cre cassette, which amplifies a 1.6 Kbp product in TG alleles. Template genomes were collected from small mouse tail tissues.

METHOD DETAILS

Voluntary activity

Control and *Ddx54*^{fl/fl}*;MBP-Cre* mice (n = 10) were singly housed after reaching 5 weeks of age. Infrared sensors (Neuroscience, Tokyo, Japan) were attached over each cage, and the activity counts of each mouse were logged under 24-h monitoring from 5 to 21 weeks of age. The daily counts were averaged over each week for each mouse to compare the voluntary activity between groups. Due to an accidental shutdown of the data collecting computer, the activity data at the age of 6 weeks are absent from the analysis.

Rotarod testing

The motor coordination of mice was assessed using a rotarod apparatus (MK-600, Muromachi Kikai, Tokyo, Japan). The rod (3 cm in diameter) was horizontally positioned at 13 cm above the floor of the apparatus and divided by 6 thin flanges (25 cm in diameter) to create 5 walking lanes (each 6 cm in width) for the mice. To train mice to walk on the rotating rod, each mouse was placed in each lane at 6 rpm 3 times, followed by 2 additional sessions on the rod rotating at 11 rpm. One day after the training, recording of time until falling off the rod was started with a constant rotating speed of 11 rpm. The cutoff time was set to 180 s for each trial, which was repeated 3 times a day with inter-trial intervals of 30 min. After each session was finished, all the walking lanes were cleaned with moistened paper towel and then wiped dry. Testing was performed once a week except for the first and second weeks of recording, during which the mice underwent the rotarod test 3 and 2 days, respectively. The latency was averaged over 3 sessions for each animal on each experimental day to evaluate motor coordination.

Y maze test

The spatial reference memory of mice was evaluated using the Y maze according to a previously reported protocol[56] with some modifications. The apparatus consisted of 3 identical arms (40 cm [L] x 5 cm [W] x 12 cm [H]) that were radially extended and 120° apart from each other. Each test consisted of an acquisition session and a testing session, both of which lasted for 5 min. In the acquisition session, a mouse was gently placed on the distal end of 1 arm (hereafter referred to as the "start arm") in the apparatus with another arm being closed off with a block, thus allowing the mouse to explore between the start arm and the remaining single arm (referred to as the "known arm"). Immediately after the acquisition session, the test mouse was gently picked up and returned to its home cage, where it remained during the 15-min inter-trial interval.

The mouse was then placed again in the start arm, in a similar way as in the acquisition session, to undergo the testing session, during which all 3 arms were accessible. After finishing each session, the apparatus was cleaned with moistened paper towel and then wiped dry. During both sessions, the exploratory behavior of mice was recorded with a CCD camera (Sony, Tokyo, Japan) attached over the maze, and analyzed with video tracking software (Limelight ver. 2, Actimetrics, IL, USA). Mice with intact spatial reference memory preferentially explore the previously inaccessible arm (referred to as the "novel arm") compared to the known arm in the testing session due to their innate curiosity.[56] Thus, the percentages of time spent and distance traveled in the novel arm were compared with those in the known arm for each genotype.

Macroscopic observation, histopathology, and Luxol fast blue staining

The mice were necropsied at 6.0–6.5 Mo and gross observation was performed for the main organs and tissues of the head, chest, and abdomen. Granular surface and atrophy of kidneys and moderate accumulation of ascitic fluid in the abdominal cavity were observed. Histopathological examination was performed on the brain, liver, kidneys, lungs, pancreas, spleen, and testis. The mice were sacrificed and perfused through the left ventricle with 4% paraformaldehyde. Brains were dissected and then post-fixed for 2 days in the original fixative before trimming into blocks for embedding in paraffin. The cerebrum, cerebellum, and brain stem were embedded in paraffin and coronal sections were stained with hematoxylin and eosin (H&E) and Luxol fast blue (LFB). The results of LFB staining are shown in Figures 1A–1D. Other organs were fixed with 15% phosphate-buffered formalin, embedded in paraffin, and sectioned, and the sections were stained with H&E. Mild atrophy was observed in the spleen and testis. In the kidneys, degeneration of renal tubules (moderate), fibrosis (mild), hyaline casts (severe), and atrophy of glomeruli (mild) were observed. These renal changes cause glomerular hyperpermeability and impaired reabsorption in the renal tubules, although they are relatively mild compared with the brain changes and not thought to be the cause of convulsions. Control mice did not develop those neurologic signs and renal changes.

Tissue lysis and immunoblotting

Tissues were lysed in lysis buffer A (50 mM Hepes-NaOH [pH 7.5], 3 mM $MgCl_2$, 150 mM NaCl, 1 mM dithiothreitol, 1 mM phenylmethane sulfonylfluoride, leupeptin [1 mg/mL], 1 mM EDTA, 1 mM Na_3VO_4, and 10 mM NaF) containing biochemical detergents (0.5% NP-40, 1% CHAPS, and 0.03% SDS). All lysis steps were performed at 4°C. The supernatants cleared by centrifugation were denatured, subjected to SDS–polyacrylamide gel electrophoresis, and transferred to polyvinylidene difluoride membranes using the TransBlot TurboTransfer System (Bio-Rad). The membranes were blocked with Blocking One (Nacalai) and immunoblotted using a primary antibody followed by a peroxidase-conjugated secondary antibody. The bound antibodies were detected using Chemiluminescence One (standard and strong detection reagents; Nacalai). The bands were scanned using a C-DiGit Blot Scanner (MS Systems) and then densitometrically analyzed for quantification using UN-SCAN-IT software (Silk Scientific). The exposed X-ray films were captured as TIFF image files using a GT-S640 scanner system (Cannon, Tokyo, Japan).

Immunohistochemistry

Two fixation protocols were used. 1) nerve tissues were directly fixed with ice-cold acetone and embedded in Tissue-Tek reagent (Sakura Finetechnical). 2) tissues were perfused with phosphate-buffered saline (PBS) and then fixed with PBS containing 4% paraformaldehyde. They were post-fixed with 4% paraformaldehyde, incubated with 20% sucrose, and embedded in Tissue-Tek reagent. Microtome (NX70; Thermo Fisher Scientific) sections were blocked with Blocking One and incubated first with a primary antibody and then with a fluorescent substance–labeled secondary antibody. Glass coverslips were mounted with Vectashield Mounting Medium (Vector Laboratories). The fluorescent images were visualized using a microscope system with a laser-scanning FV1000D or FV1200 apparatus (Olympus, Tokyo, Japan) or BZX-710 fluorescent microscope (Keyence, Osaka, Japan). Image analyses were conducted using BZ-X Analyzer (Keyence). Images in figures are representative of 3–6 independent experimental results or mice.

Electron microscopy

For electron microscopy, nerve tissues were fixed with 2% paraformaldehyde and 2% glutaraldehyde in 0.1% cacodylate buffer, contrasted with 2% osmium tetroxide, dehydrated with an ethanol gradient, and treated with propylene oxide. Finally, samples were infiltrated and embedded in pure epoxy. Ultrathin sections (Ultracut UCT; Leica) were stained with uranyl acetate and lead staining solution. Images were taken with a JEM-1200EX or JEM-1400 Plus electron microscope system (JEOL) by Tokai Electron Microscopy,

Inc. (Nagoya, Japan). The g-ratio is the ratio of axon diameters to the outer myelinated axon diameters. These ratios were used to generate graphs for axon diameter, and their distributions were also shown in the graph.

TUNEL assay

Assays were performed using a TACS·XL-Blue Label *in Situ* Apoptosis Detection kit according to a protocol adapted from the manufacturer (Trevigen, Inc., Gaithersburg, MD, USA). TUNEL-positive cells were quantified by counting within the corpus callosum. Only those TUNEL+ cells with an observable nucleus by DAPI staining were counted.

Cuprizone experiment

Mice were divided into the following 4 groups at the age of 8 weeks: i.e., Control-vehicle, Control-cuprizone, *Ddx54*^{fl/fl};*MBP-Cre*-vehicle, and *Ddx54*^{fl/fl}; *MBP*-Cre-cuprizone groups. After 1-week acclimatization, the vehicle groups were fed powdered diet; the cuprizone-treated groups were fed powdered diet with 0.2% (w/w) cuprizone (Kanto Chemical, Tokyo, Japan) for 5 weeks, after which some mice in each group were sacrificed for the immunohistochemical and electron-microscopic analyses of demyelination. All the remaining mice were fed normal powdered diet for an additional 2 weeks and then sacrificed to examine the extent of the remyelinating ability in each cuprizone group.[57]

Oligodendrocyte-neuronal co-cultures

Oligodendrocyte precursor cells were isolated from embryonic day 15 (E15) Sprague-Dawley (SD) rats as described previously.[55] Briefly, cerebral cortices were dissected, dissociated with 0.25% trypsin, triturated, and passed through mesh with 70-μm pores. Cells were collected, resuspended in MEM containing 10% FBS, 50 U/ml penicillin, and 50 μg/mL streptomycin, and seeded on poly-L-lysine-coated dishes. After 2 passages, the cells were cultured on non-coated Petri dishes (Thermo Scientific). On the second day of culture, the medium was changed to a DMEM-based serum-free growth medium containing PDGF-AA and bFGF (Peprotech, Rocky Hill, NJ, USA) and N2 (Thermo Scientific), and the cells were cultured for an additional 2 days. These cells were then used as oligodendrocyte precursor cells. Primary neurons were dissociated from mouse dorsal root ganglia (DRGs) as described elsewhere. DRG neurons were purified by culturing on collagen-coated dishes or wells (AGC Techno Glass) in DMEM-GlutaMAX I (Thermo Fisher Scientific) containing 10% heat-inactivated FBS, 100 ng/mL NGF, 8 μM fluorodeoxyuridine, and 4 μM uridine in 5% CO_2 at 37°C. After 3 cycles of antimitotic reagent administration over 2 to 3 weeks, purified neurons were cultured in DMEM-GlutaMAX I containing 10% FBS and 100 ng/mL NGF. To confirm cell viability under these experimental conditions, and the percentage of attached, trypan-blue-incorporating cells was below 5% in each culture. Co-cultures were established by seeding ∼100,000 purified oligodendrocyte precursor cells on neurons. Co-cultures were maintained for 4 weeks and the medium was replaced every 3 to 4 days.

Preparation of plasmids containing short hairpin RNAs (shRNAs)

All nucleotide sequences were confirmed by sequencing. The sense antisense oligonucleotides, which were used for duplex production, were as follows. The sequences of Ddx54#1 (starting from nucleotide 348 of rat Ddx54) shRNA, Ddx54#2 (starting from nucleotide 585 of rat Ddx54) and the control Photinus pyralis luciferase shRNA were presented in key resources table. The annealed duplexes were ligated into the retrovirus vector, pSINmU6 (Takara Bio, Shiga, Japan).

Production of retroviruses and retrovirus-mediated DNA transfection

Using a CalPhos Transfection kit (Takara Bio), each retrovirus vector was co-transfected into G3Thi cells with vectors pVSVG and pGP, which were provided with the Takara Bio retroviral production kit. After 2 days, each culture supernatant was centrifuged at 10,000 rpm for 8 h to concentrate the recombinant retroviruses. The virus pellets were suspended in each culture medium. Since retroviruses are infected into proliferating cells, they were used for infection into growing, primary oligodendrocyte precursor cells before being co-cultured with neurons.

Effect of an herbal medicine on *Ddx54*^{fl/fl};*MBP-Cre* mice

Yokukansankachinpihange (TJ-83) is a traditional Japanese herbal medicine composed of 9 medicinal plants and is used to improve neurosis, insomnia in adults, and night crying in children. A pharmaceutical

grade TJ-83 (Tsumura & Co., Tokyo, Japan), an ethical drug approved by Ministry of Health, Labor and Welfare of Japan, was mixed into the diet at a concentration of 2% and the mice consumed this diet up to the age of 9 weeks.

QUANTIFICATION AND STATISTICAL ANALYSIS

Methods of quantitation are described in the paragraphs of each experiment in "method details" section. Methods of statistical analysis are described in the figure legends. Software used included Excel (ver. 2019, Microsoft, Redmond, WA), StatPlus (ver. 5, AnalystSoft, Walnut, CA), GraphPad Prism (ver. 9, San Diego, CA) and R ver 2.8.1 (R core team).